Self-ubiquitination of a pathogen type-III effector traps and blocks the autophagy machinery to promote disease

Jia-Xuan Leong[1], Margot Raffeiner[2], Daniela Spinti[2], Gautier Langin[1], Mirita Franz-Wachtel[3], Andrew R. Guzman[4], Jung-Gun Kim[4], Pooja Pandey[5], Alyona E. A. Minina[6], Boris Macek[3], Anders Hafrén[7], Tolga O. Bozkurt[5], Mary Beth Mudgett[4], Frederik Börnke[2,8], Daniel Hofius[7], Suayib Üstün[1*]

[1]University of Tübingen, Center for Plant Molecular Biology (ZMBP), 72076 Tübingen, Germany
[2]Leibniz-Institute of Vegetable and Ornamental Crops (IGZ), 14979 Großbeeren, Germany
[3]Interfaculty Institute for Cell Biology, Department of Quantitative Proteomics, University of Tübingen, 72076 Tübingen, Germany.
[4]Department of Biology, Stanford University, Stanford, CA 94305, USA
[5]Department of Life Sciences, Imperial College London, SW7 2AZ London, United Kingdom.
[6]Department of Molecular Sciences, Uppsala BioCenter, Swedish University of Agricultural Sciences and Linnean Center for Plant Biology, 75007 Uppsala, Sweden.
[7]Department of Plant Biology, Uppsala BioCenter, Swedish University of Agricultural Sciences and Linnean Center for Plant Biology, 75007 Uppsala, Sweden.
[8]Institute of Biochemistry and Biology, University of Potsdam, 14476 Potsdam, Germany

Keywords: Autophagy, Effectors, Immunity, Ubiquitination, Disease, Xenophagy

*corresponding author
suayib.uestuen@zmbp.uni-tuebingen.de

Abstract:

Beyond its role in cellular homeostasis, autophagy is considered to play anti- and pro-microbial roles in host-microbe interactions, both in animals and plants. One of the prominent roles of anti-microbial autophagy in animals is to degrade intracellular pathogens or microbial molecules, in a process termed "xenophagy". Consequently, microbes evolved mechanisms to hijack or modulate autophagy to escape elimination. However, the extent to which xenophagy contributes to plant-bacteria interactions remains unknown. Here, we provide evidence that NBR1/Joka2-dependent selective autophagy functions in plant defence by degrading the bacterial type-III effector (T3E) XopL from *Xanthomonas campestris* pv. *vesicatoria (Xcv)*. We show how XopL associates with the autophagy machinery and undergoes self-ubiquitination, subsequently triggering its own degradation by the NBR1/Joka2-mediated selective autophagy. Intriguingly, *Xcv* is also able to suppress autophagy in a T3E-dependent manner by utilizing the same T3E XopL that interacts and degrades the autophagy component SH3P2 via its E3 ligase activity. Thus, XopL is able to escape its own degradation and promote pathogenicity of *Xcv* by inhibiting autophagy through SH3P depletion. Together, we reveal a novel phenomenon how NBR1/Joka2 contributes to anti-microbial autophagy that we termed "effectorphagy". We provide a unique mechanism how a T3E undergoes self-modification to act as a bait to trap host cellular degradation machineries.

Significant statement

Autophagy has anti- and pro-microbial roles in host-microbe interactions. Its anti-microbial role is derived from its ability to degrade intracellular pathogens, termed “xenophagy”. The contribution of xenophagy to host-bacteria interactions in plants and its substrates remains elusive. Here, we reveal that NEIGHBOR OF BRCA1 (NBR1)-mediated autophagy has an anti-microbial role towards bacteria by degrading the type-III effector (T3E) XopL from *Xanthomonas campestris* pv. *vesicatoria (Xcv),* a process we termed “effectorphagy”. We unveil that the same T3E is able to perturb autophagy to escape its own degradation and to boost bacterial virulence. These findings highlight a novel role of xenophagy that is conserved across kingdoms and we offer new perspectives on how T3Es undergo self-modification to trap host cellular degradation pathways.

Introduction

Eukaryotic cells react dynamically to external and internal stimuli by adjusting their proteome. This requires a stringent regulation of protein homeostasis which is achieved by regulated protein degradation. Cellular degradation machineries including the proteasome and autophagy maintain protein homeostasis by recycling unwanted or dysfunctional proteins (1). While the proteasome degrades short-lived proteins or mis-folded proteins, autophagy can remove larger protein complexes, insoluble aggregates, entire organelles as well as pathogens. Under normal conditions, both degradation pathways are critical for cellular housekeeping functions, while under stress conditions they facilitate the reorganization of the proteome to adapt to a changing environment (2).

Regulated proteolytic degradation by proteasome has been identified as an essential component of immunity influencing the outcome of host-microbe interactions in across kingdoms (3, 4). In the recent years, autophagy has also emerged as a central player in immunity and disease in humans and plants (5-9). In mammals, autophagy has various connections to a number of diseases, regulating cell death and innate immunity (7, 10). Dual roles have also been ascribed to autophagy in host-bacteria interactions (11). While some bacterial pathogens recruit the autophagy machinery in order to create a replicative niche (pro-bacterial autophagy), anti-bacterial autophagy removes bacterial intruders to limit pathogen infection (12). The elimination of bacteria is a selective autophagy response, termed xenophagy (13). In this process, bacterial pathogens such as *Salmonella* and *Shigella* are degraded by autophagy through a ubiquitin-dependent mechanism (14, 15). This demonstrates that autophagy is not only a largely unspecific ("bulk") catabolic and recycling process, as increasing evidence now indicates that autophagy also acts as a selective mechanism to degrade protein aggregates, organelles and pathogens. Selectivity is mediated by autophagy receptors, of which p62 and NBR1 play key roles in controlling pathogenic infection in mammals (13). Both autophagy receptors can bind to ubiquitinated bacteria, and degrade them, through their ability to bind autophagosome-associated ATG8 proteins (13).

Plants possess a homologue of NBR1 that was recently described to be involved in plant immunity. Plant NBR1, which is also referred as Joka2 in solanaceous species, is able to restrict growth and disease progression of the plant pathogenic oomycete *Phytophthora infestans*, the bacterium *Pseudomonas syringae* pv. *tomato (Pst)*, and plant viruses such as turnip mosaic virus (TuMV) and cauliflower mosaic virus (CaMV) (16-20). These studies demonstrated that, similar to that in mammals, plant NBR1 participates in xenophagy by degrading viral proteins. Whether NBR1-mediated xenophagy also plays a role in plant-bacteria interactions remains to be determined. This is complicated by the fact that bacteria reside in the extracellular spaces of plant tissues and might not be directly targeted by xenophagy.

It is known that type-III effector (T3E) proteins of plant pathogenic bacteria are present in the host cell. These effectors are able to manipulate host defense responses for the benefit of the pathogen (21). Very recently, it has been shown that microbial effectors perturb or hijack degradation machineries to attenuate plant immune reactions (22, 23). For instance, *Pst* activates autophagy via the action of the T3E HopM1 to degrade the proteasome and suppress its function in a process termed proteaphagy (18, 24). Although this process can be categorized as a pro-bacterial role of autophagy, NBR1-mediated anti-bacterial autophagy seems to restrict lesion formation and pathogenicity of *Pst* (25). The dual role of autophagy in plant-bacteria interactions is further confirmed by findings that certain effectors are also able to suppress autophagy responses, although the understanding of the exact molecular mechanisms are still very limited (26).

Like *Pst*, *Xanthomonas campestris* pv. *vesicatoria (Xcv)* is another well-studied hemi-biotrophic bacterium, causing disease on tomato and pepper plants (27). Mounting evidence has been established that *Xcv* and its T3Es exploit plant ubiquitin- and ubiquitin-like pathways (28, 29). While the role of the proteasome system in *Xanthomonas* infections is well understood,

little is known about how autophagy shapes the outcome of *Xanthomonas*-host interactions. Recent findings in the cassava- *Xanthomonas axonopodis* pv. *manihotis* (*Xam*) model suggest that autophagy has an anti-bacterial role *(30, 31)*. However, our current understanding about how T3Es might modulate and regulate this response is very limited. Are there similar mechanisms operating in pro- and antibacterial roles across different pathogenic bacteria? Do plants utilize xenophagy as an anti-bacterial mechanism to degrade pathogenic components in plant-bacteria interactions?

To address these questions, we performed a mechanistic analysis of the interplay of plant autophagy and *Xcv* pathogenesis. Here, we provide evidence that NBR1/Joka2 degrades T3E XopL, which undergoes self-ubiquitination *in planta*. However, *Xcv* utilizes the same T3E XopL to dampen autophagy by degrading autophagy component SH3P2 in a proteasome-dependent manner via its E3 ligase activity. This rescues T3E XopL from being targeted for degradation by the selective autophagy receptor NBR1/Joka2 and enhances the virulence of *Xcv* in plants. We provide a novel example of how a bacterial T3E traps the autophagy pathway by self-ubiquitination and targeting itself to the NBR1-mediated selective autophagy pathway, a process we term “effectorphagy”.

Results

Xanthomonas blocks autophagy in an effector-dependent manner to promote pathogenicity

Given the prominent role of autophagy in host-microbe interactions, we investigated different autophagy responses after Xanthomonas infection. To this end we used the model plant *Nicotiana benthamiana*, as Agrobacterium-mediated transient expression, Virus-induced gene silencing (VIGS), autophagy assays and the use of antibodies are well established and reproducible. Assays were conducted with a *Xcv* strain harboring a deletion in the T3E XopQ (*Xcv ΔxopQ)*, which is a host range determinant in *Nicotiana* species (32). In the absence of XopQ, *Xcv* is fully virulent in *Nicotiana benthamiana* leaves. First, we utilized a quantitative autophagy assay to measure autophagic turnover during infection. This assay is based on Agrobacterium-mediated transient expression of *Renilla* luciferase (RLUC) fused to ATG8a (RLUC-ATG8a) or NBR1 (RLUC-NBR1) together with free *Firefly* luciferase (FLUC) in *N. benthamiana* leaves, which serves as an internal control (18, 33). We also used the previously described autophagy suppressor AIMp, derived from the *Phytophthora* PexRD54 effector (34), as a control for autophagy suppression. Simultaneous measurements in the dual-luciferase system revealed that *Xcv ΔxopQ* infection in leaves expressing the autophagy reporters led to a significant increase of RLUC-ATG8a/FLUC and RLUC-NBR1/FLUC ratios normalized to mock, suggesting reduced autophagic turnover (Fig. 1A). This is the first indication that *Xanthomonas* infection blocks autophagic turnover *in planta*. To support our data from the quantitative dual-luciferase flux assay we monitored autophagosome formation using RFP-ATG8G that decorates autophagosomes (18). We infected *N. benthamiana* plants transiently expressing RFP-ATG8G with *Xcv ΔxopQ* and monitored the formation of autophagosomes in the presence or absence of Concanamycin A (ConA). ConA is an inhibitor of vacuolar acidification that blocks autophagic body degradation (35, 36). In the absence of ConA, *Xcv ΔxopQ* induced massive accumulation of autophagosome-like structures which could not be further enhanced by the presence of ConA (Fig. 1B). This confirmed our finding that *Xcv* modulates autophagic degradation *in planta*. The induction of autophagosome formation and suppression of autophagic degradation prompted us to investigate host autophagy by immunoblotting for endogenous ATG8 and Joka2 in *N. benthamiana* (16, 35). Joka2 protein abundance increased during infection, to a small extent 1-day post-inoculation (dpi), and to a greater extent at 2 dpi, while ATG8 protein levels only slightly increased at 2 dpi (Fig. 1C). Another indicator of impaired autophagy is the increased gene expression of the autophagic markers (36). Transcript levels of *Joka2*, *NbATG8-2.1/2* and *NbATG8-1.1/2* were significantly

higher compared to mock infection at 2 dpi (Fig. 1D), with *NbATG8-2.1/2* showing an earlier increase than the two other genes. To assess the relevance of suppressed autophagic degradation during infection, we determined bacterial growth in plants transiently expressing the autophagy suppressor AIMp. At 6 dpi, *Xcv* growth was significantly elevated in *N. benthamiana roq-1* plants (37) transiently expressing RFP-AIMp compared to empty vector (EV) control (Figure 1E). The same trend was observed when *ATG7* was silenced using virus-induced gene silencing (VIGS) in *N. benthamiana* as silencing of *ATG7* rendered plants more susceptible to *Xcv* Δ*xopQ* at 6 dpi (Fig. S1). Because T3Es were previously shown to modulate proteasome function and autophagy (18, 24, 26, 38), we also analyzed the autophagy responses to a nonpathogenic type-III secretion system (T3SS) mutant *Xcv ΔhrcN*, which is unable to drive secretion of T3Es (39). In contrast to *Xcv ΔxopQ*, the T3SS-deficient mutant *Xcv ΔhrcN* did not alter the RLUC-ATG8a/FLUC or RLUC-NBR1/FLUC ratio, nor protein abundance of ATG8 and Joka2 (Fig. S2A and B). Consistent with this, gene expression analysis also revealed no significant induction of the autophagy marker genes *Joka2* and *NbATG8-1.1/2* (Fig S2C). Together, these data support the model that *Xcv* blocks autophagy in a T3E-dependent manner to promote virulence.

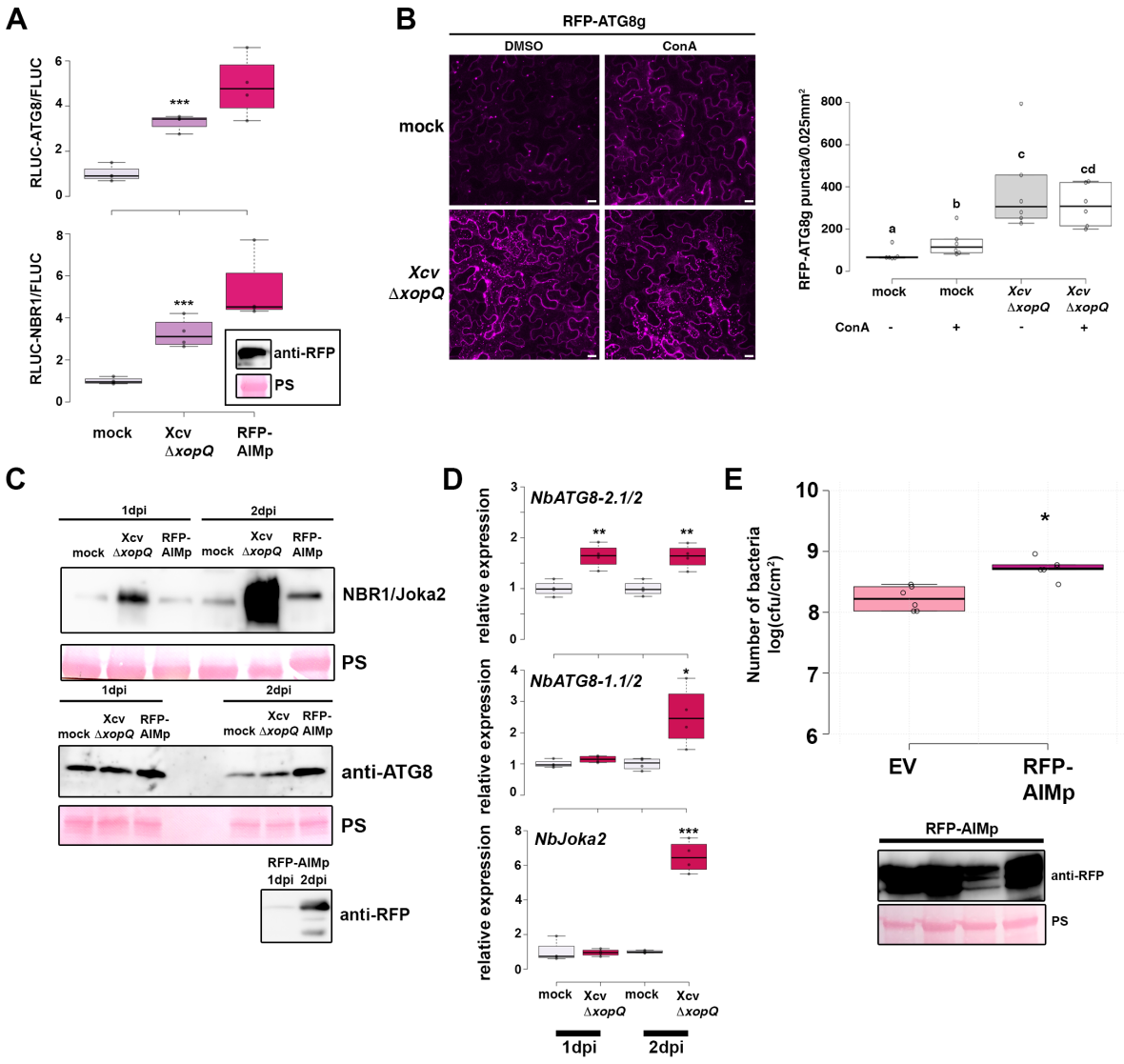

Figure 1: Xanthomonas blocks autophagy to enhance its pathogenicity

(A) Autophagic flux determined by quantitative dual-luciferase assay. RLUC-ATG8a or RLUC-NBR1 constructs were coexpressed with internal control FLUC in *N. benthamiana*. *Xcv*

ΔxopQ was co-infiltrated with Agrobacteria containing the Luciferase constructs. Coexpression of RFP-AIMp serves as a control for autophagy inhibition. Expression of the latter was confirmend with western blot (inset). Renilla (RLUC) and Firefly (FLUC) luciferase activities were simultaneously measured in leaf extracts at 48 h post- infiltration using the dual-luciferase system. Values represent the mean ratio of RLUC-ATG8a and FLUC activities and error bars show SD (n=4). Statistical significance (***P<0.001) was revealed by Student's *t*-test. The experiment was repeated more than 3 times with similar results.
(B) RFP-ATG8g-labeled autophagosomes were quantified from plants infected with mock or Xcv *ΔxopQ* at 2 dpi in the presence or absence of ConA (bars = 20 µm). Puncta were calculated Puncta were calculated from z-stacks (15) of n=6 individuals using ImageJ. Center lines show the medians; box limits indicate the 25th and 75th percentiles as determined by R software; whiskers extend 1.5 times the interquartile range from the 25th and 75th percentiles and data points are plotted as open circles. Different letters indicate statistically significant differences ($P < 0.05$) as determined by one way ANOVA. The experiment was repeated twice with similar results.

T3E XopL suppresses autophagy

To address which T3E(s) might manipulate autophagy, we used the quantitative dual-luciferase autophagy assay. We screened for *Xcv* T3Es XopJ, XopD and XopL with known function in proteolytic degradation pathways (28, 40-43) as well as XopS which has not been described to degradation machineries. Measurement of luciferase activities showed that the transient expression of XopL, a previously characterized E3 ligase (41), led to a significant increase in RLUC-ATG8a/FLUC and RLUC-NBR1/FLUC ratio (Fig. 2A), which was consistent across multiple experiments. In contrast, transient expression of XopD and XopS had no evident effect in the luciferase assay, while XopJ also significantly impacted autophagy (Fig. S3A). This may be due to its inhibitory effect on the proteasome (38), as MG132 (a proteasome inhibitor) treatment also results in an increase of the RLUC-ATG8a/FLUC ratio (Fig S3B). Performing immunoblot analysis of ATG8 protein levels in *N. benthamiana* leaves, we found that transient expression of XopL resulted in an accumulation of NBR1 and ATG8 proteins. This could not be further increased by ConA treatment in the case of ATG8 (Fig. 2B and C).
To validate that XopL also acts as an autophagy suppressor during *Xcv* infection we constructed a *xopL* deletion mutant in *Xcv ΔxopQ*. The deletion mutant displayed reduced growth and symptom development upon infection of tomato plants and in *N. benthamiana* (Fig S4), demonstrating that XopL is an essential virulence factor. Utilizing our quantitative dual-luciferase autophagy assay, we discovered that *Xcv ΔxopQ ΔxopL* was unable to suppress autophagy to levels observed in tissues infected with *Xcv ΔxopQ* levels (Fig. 2D), indicating that XopL has a major impact on autophagy during infection. However, *Xcv ΔxopQ ΔxopL* still leads to a slight increase in both RLUC-ATG8a/FLUC and RLUC-NBR1/FLUC ratios, suggesting that *Xcv* possesses another T3E with a redundant function. By analyzing ATG8 and NBR1 protein levels, we also verified that XopL partially contributes to an increase in ATG8 and NBR1 accumulation (Fig. 2E), supporting the notion that XopL suppresses autophagic degradation during infection. To analyze whether XopL has similar functions in other plant species, we generated transgenic *Arabidopsis thaliana* lines expressing GFP-XopL under the UBQ10 promoter. Confocal microscopy analysis revealed that GFP-XopL localizes to punctate structures in *A. thaliana* leaf epidermal cells (Fig. S5C). Further analysis of GFP-XopL transgenic *A. thaliana* plants revealed that NBR1 protein abundance in the absence and presence of ConA treatment is drastically increased (Fig. S5A), suggesting a block of NBR1 turnover. The early senescence phenotype of transgenic lines expressing XopL (Fig. S5B) and elevated gene expression of ATG8a and NBR1 is also indicative of altered autophagy responses (Fig. S5D).

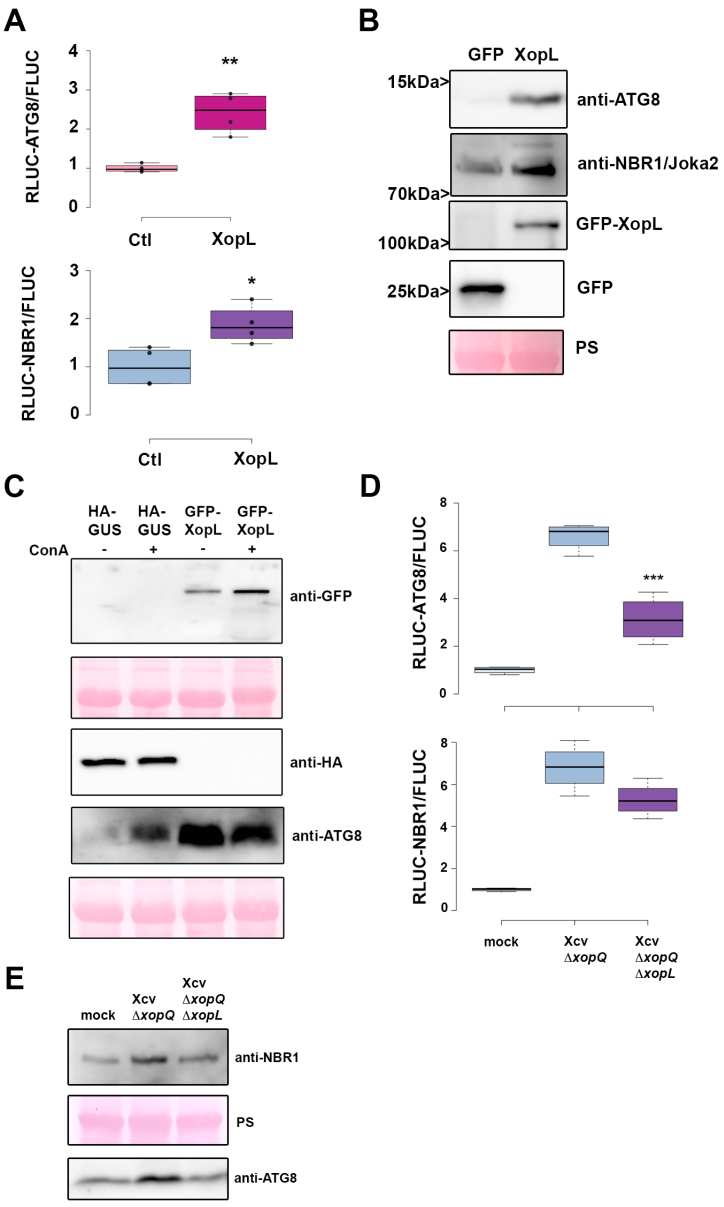

Figure 2: Xanthomonas T3E XopL is suppressing autophagy

(A) RLUC-ATG8a or RLUC-NBR1 constructs were coexpressed with internal control FLUC in *N. benthamiana*. XopL or control (Ctl) constructs were co-infiltrated. RLUC and FLUC activities were simultaneously measured in leaf extracts at 48 h post- infiltration using the dual-luciferase system. Values represent the mean ratio of RLUC-ATG8a and FLUC activities and error bars show SD (n=4). Statistical significance (* $P < 0.5$, ** $P < 0.01$) was revealed by Student's *t*-test. The experiment was repeated more than 3 times by 2 different people with similar results.

(B) Immunoblot analysis of NBR1 and ATG8 protein levels in *N. benthamiana* plants transiently expressing GFP-XopL or GFP control at 2dpi. Expression of GFP-XopL and GFP were verified with an anti-GFP antibody. Ponceau Staining (PS) served as a loading control. T The experiment was repeated at least three times by 2 different people with similar results.

(C) Immunoblot analysis of NBR1 and ATG8 protein levels in *N. benthamiana* plants transiently expressing XopL or GUS control at 2dpi in the presence or absence of ConA. Expression of GFP-XopL was verified with an anti-GFP antibody, while expression of GUS-HA was confirmed with an anti-HA antibody. Ponceau Staining (PS) served as a loading control. The experiment was repeated twice with similar results.

(D) RLUC-ATG8a or RLUC-NBR1 constructs were coexpressed with internal control FLUC in *N. benthamiana*. Xcv *ΔxopQ and* Xcv *ΔxopQ ΔxopL* were co-infiltrated with Agrobacteria containing the respective constructs. RLUC and FLUC activities were simultaneously measured in leaf extracts at 48 h post- infiltration using the dual-luciferase system. Values represent the mean ratio of RLUC-ATG8a and FLUC activities and error bars show SD (n=4). Statistical significance (***$P < 0.001$) was revealed by Student's *t*-test. The experiment was repeated 3 times with similar results.
(E) Immunoblot analysis of NBR1 and ATG8 protein levels in Xcv *ΔxopQ,* Xcv *ΔxopQ ΔxopL* or mock infected *N. benthamiana* plants at 2dpi. Ponceau Staining (PS) served as a loading control. The experiment was repeated twice with similar results.

NBR1/Joka2-mediated selective autophagy degrades ubiquitinated XopL

Our findings demonstrate that *Xcv* not only blocks bulk autophagy but also NBR1/Joka2-dependent selective autophagy. Previous studies imply that NBR1/Joka2 mediates xenophagy by degrading viral particles and that Joka2 is required for immunity against bacteria and *Phytophthora* (16, 18, 20, 44). Plant NBR1 is a hybrid of the mammalian autophagy adaptors NBR1 and p62/SQSTM1 (35). The latter was shown to mediate xenophagy of *Mycobacterium tuberculosis* (Mtb) by binding to the Mtb ubiquitin-binding protein Rv1468c and ubiquitin-coated *Salmonella enterica* in human cells (45, 46). However, the mode of action and targets of plant NBR1 during microbial infection remain elusive. Revisiting our previous results, we realized that the abundance of XopL increased when we blocked vacuolar degradation with ConA (Fig. 2C), which is also true for *A. thaliana* plants stably expressing XopL (Fig S5A) or *N. benthamina* leaves expressing both XopL and the autophagy suppressor AIMp (Fig. 3A). To further validate if XopL undergoes autophagic degradation in the vacuole, we used a transgenic line *A. thaliana* expressing GFP-XopL treated with ConA to block vacuolar turnover. Confocal microscopy was performed in root cells as vacuolar degradation is easier to assess in this tissue. We observed multiple GFP-labeled structures reminiscent of autophagic bodies in root vacuoles of ConA-treated seedlings compared to the control (Fig. S6). As autophagic degradation of viral proteins and animal pathogenic bacteria is mediated by NBR1, we decided to examine whether XopL and NBR1 associate *in planta*. Intriguingly, we discovered that XopL co-localizes with NBR1 in puncta and in large aggregate-like structures (Fig. 3B), suggesting that NBR1 associates with XopL *in planta*. Association of both proteins was determined using Förster resonance energy transfer by fluorescence lifetime imaging microscopy (FRET-FLIM). Only in the presence of RFP-XopL a significant reduction of 0.1 ns in the lifetime of the donor Joka2 was observed in comparison to co-expression of RFP or donor alone (Fig. 3C). These findings prompted us to investigate whether XopL might be targeted by NBR1/Joka2 for autophagic degradation, similar to insoluble ubiquitinated protein aggregates (47). Performing pull-down experiments with GFP-XopL, we discovered that XopL associates with NBR1/Joka2 *in planta* (Fig. 3D), confirming the results of our co-localization study. To address whether E3 ligase activity of XopL is required for interaction, we employed the triple point mutant of $XopL_{H584A\ L585A\ G586E}$ (hereafter referred to as XopL ΔE3), lacking E3 ligase activity (41, 54). Co-IP experiments revealed that XopL ΔE3 was also able to pull-down NBR1/Joka2 after transient expression in *N. benthamiana* (Fig. 3E). This suggests that NBR1/Joka2 may not mediate the degradation of a complex containing XopL and its ubiquitinated target protein(s), but rather targets XopL for autophagic degradation. Given the fact that XopL is degraded by autophagy and associates with NBR1/Joka2, we next analyzed stability of XopL in Joka2 silenced *N. benthamiana* plants. Silencing of NBR1/Joka2 was confirmed by qPCR (Fig. S7). Indeed, we could observe an increase in XopL protein abundance in pTRV2-Joka2 plants (Fig. 3F), arguing for a direct participation of NBR1/Joka2 in XopL turnover. To assess whether this might impact pathogenicity of *Xcv* we performed bacterial growth assays using the pTRV2-Joka2 plants. Increased growth at 3 dpi and 6dpi of *Xcv ΔxopQ* in *N. benthamiana* plants silenced for Joka2

strengthened our finding that Joka2 is having anti-bacterial effects on *Xcv ΔxopQ* (Fig. 3G). As NBR1/Joka2 or p62 recognize their cargos by their ability to bind ubiquitinated substrates, we hypothesized that XopL might be ubiquitinated *in planta*. To test this, we transiently expressed GFP-XopL in *N. benthamiana* leaves and then immunoprecipitated GFP-XopL from leaf protein extracts. Ubiquitinated GFP-XopL was detected using immunoblotting and anti-ubiquitin sera. GFP-XopL, but not the GFP control, displayed polyubiquitination *in planta*, while GFP-XopL ΔE3 showed reduced polyubiquitination (Fig. 3H). To further confirm the ubiquitination of XopL, we purified total ubiquitinated proteins using the ubiquitin pan selector, which is based on a high-affinity single domain antibody that is covalently immobilized on cross-linked agarose beads. Since XopL is stabilized by the autophagy suppressor AIMp, we co-expressed XopL together with AIMp. We detected a faint smear of high-molecular weight XopL, which was strongly enhanced when co-expressed with AIMp but absent in the GFP control (Fig. 3I). To identify ubiquitinated residues within the XopL protein, we immunoprecipitated GFP-XopL from *N. benthamiana* leaves transiently expressing GFP-XopL and performed mass spectrometry (MS) analysis. *In planta* MS analysis revealed one potential ubiquitination site at lysine 191 (K191) in the N-terminal part of XopL (Fig. S8). For plant E3 ligases such as PUB22, it has been reported that its stability is dependent on its autoubiquitination activity (48). Using MBP-XopL in an *in vitro* ubiquitination assay we confirmed self-ubiquitination (Fig. S9A), indicated by the presence of higher molecular weight bands probing with an anti-MBP. Preforming LC-MS/MS we did detect the same ubiquitination (K191) site identified *in planta* when we analyzed *in vitro* ubiquitination samples containing GST-XopL (Fig. S9B). This strongly argues for an autoubiquitination of XopL. However, we cannot rule out trans-ubiquitination by plant E3 ligases, as XopL ΔE3 still interacts with NBR1 and is still ubiquitinated in *planta*, although to a lesser extent. This is strengthened by our findings showing that the mutation of lysine 191 to alanine (K191A) rendered the XopL K191A more stable than WT XopL (Fig. 3J) without altering its subcellular localization (Fig. S10) but did not abolish ubiquitination of XopL and association with NBR1/Joka2 (Fig. 3K). This might indicate the presence of additional ubiquitination sites in XopL. Taken together, our results suggest that XopL is ubiquitinated *in planta* and subjected for NBR1/Joka2-dependent selective autophagy.

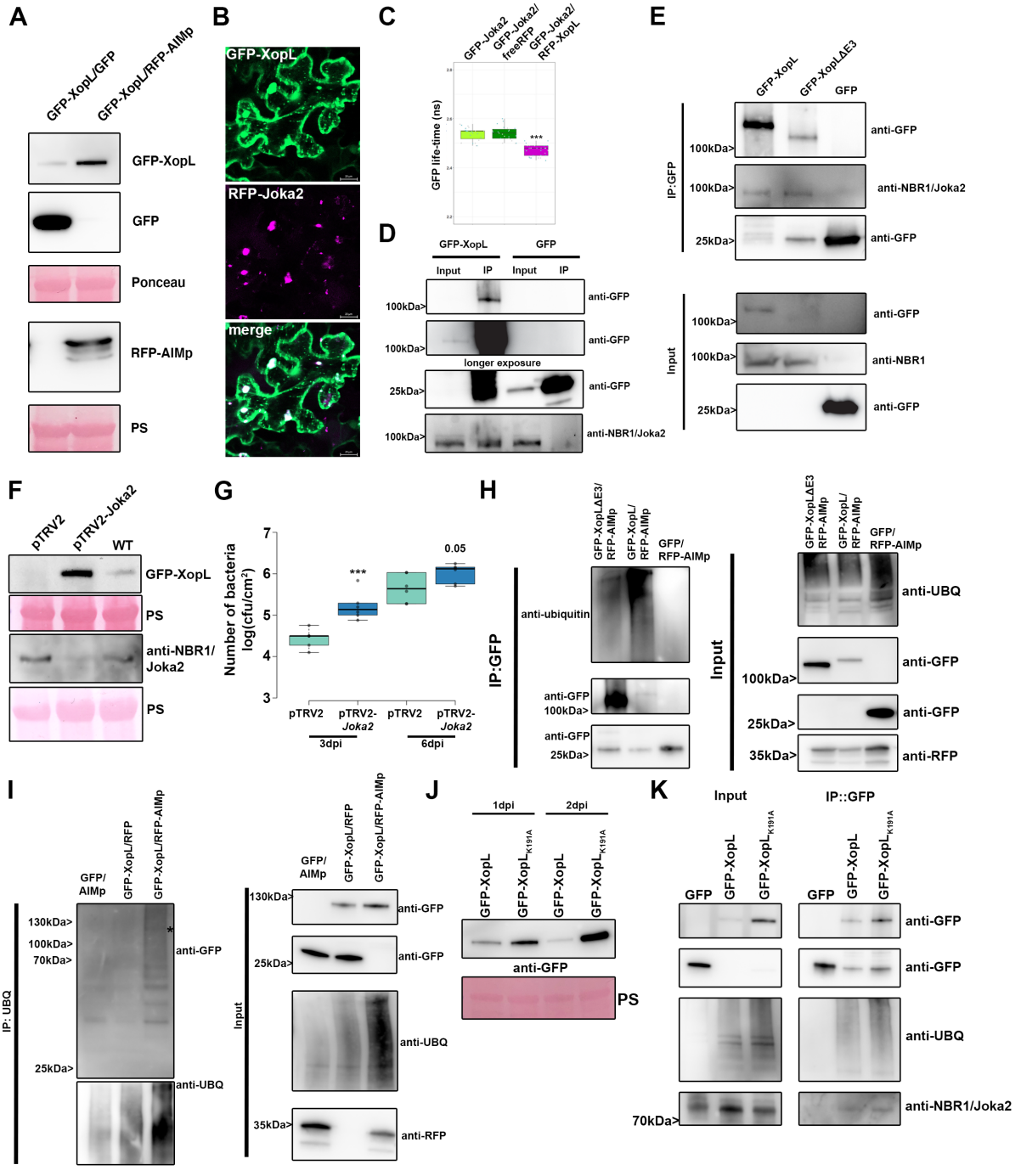

Figure 3: XopL is ubiquitinated in planta and degraded by NBR1-mediated selective autophagy

(A) Autophagy suppression enhances XopL stability. GFP-XopL was coexpressed with GFP or RFP-AIMp. Proteins were separated by SDS-PAGE and detected by immunoblotting using the indicated antibodies. Ponceau Staining (PS) served as a loading control. The experiment was repeated three times by two different people with similar results.

(B) Colocalization of GFP-XopL with RFP-Joka2 in *N. benthamiana* leaves. Imaging was performed 2 d after transient expression and images represent single confocal planes from abaxial epidermal cells (bars = 20 µm). The experiment was repeated twice with similar results.

(C) FRET FLIM measurements of GFP-Joka2 and RFP-XopL in *N. benthamiana* leaves. The freeRFP construct served as a negative control. The lifetime (in ns) of GFP-Joka2 (donor, n=27) was significantly reduced in the presence of RFP-XopL (n=29) but not in the presence of freeRFP (n=23). Scattered points show individual data points, colour indicates biological

repeats. Significant differences were calculated using Student's *t-test* and are indicated by: ***, P < 0.001.The experiment was repeated twice with similar results.
(D) Immunoprecipitation (IP) of GFP-XopL reveals association with NBR1. Immunoblots of input and IP samples from *N. benthamiana* plants transiently expressing GFP or GFP-XopL were probed with anti-GFP and anti-NBR1 antibodies.
(E) Immunoprecipitation (IP) of GFP-XopL and GFP-XopL ΔE3 reveals association with NBR1. Immunoblots of input and IP samples from *N. benthamiana* plants transiently expressing GFP, GFP-XopL and GFP-XopL ΔE3 were probed with anti-GFP and anti-NBR1 antibodies.
(F) Stability of XopL is increased in Joka2 silenced plants. GFP-XopL was transiently expressed in pTRV2, pTRV2-Joka2 and *N. benthamiana* WT plants. Expression of binary constructs was verified with an anti-GFP antibody. Joka2 silencing was verified using an anti-NBR1 antibody. Ponceau Staining (PS) served as a loading control. The experiment was repeated twice with similar results.
(G) Growth of Xcv *ΔxopQ* in *N. benthamiana* plants silenced for *Joka2* (pTRV2-Joka2) compared to control plants (pTRV2). Leaves were dip-inoculated with a bacteria suspension at OD_{600} = 0.2. and bacteria were quantified at 3 and 6 dpi. Data represent the mean SD (n = 6). Significant differences were calculated using Student's *t-test* and are indicated by: ***, P < 0.001. The experiment was repeated three times with similar trends.
(H) XopL is ubiquitinated *in planta*. GFP-XopL, GFP-XopL ΔE3 were transiently expressed in *N. benthamiana*. RFP-AIMp was co-infiltrated to stabilize both XopL variants. Samples were taken 48 hpi, and total proteins (Input) were subjected to immunoprecipitation (IP) with GFP-Trap beads, followed by immunoblot analysis of the precipitates using either anti-GFP or anti-ubiquitin antibodies. GFP served as a negative control. RFP-AIMp expression was verified by an anti-RFP antibody. The experiment was repeated three times with similar results.
(I) XopL is ubiquitinated *in planta*. GFP-XopL was transiently expressed in *N. benthamiana*. RFP-AIMp was co-infiltrated to stabilize GFP-XopL. Samples were taken 48 hpi, and total proteins (Input) were subjected to immunoprecipitation (IP) with the ubiquitin pan selector, followed by immunoblot analysis of the precipitates using either anti-GFP or anti-ubiquitin antibodies. GFP served as a control. RFP-AIMp expression was verified by an anti-RFP antibody. Asterisk indicates the GFP-XopL full-length protein. The experiment was repeated three times with similar results.
(J) Immunoblot analysis GFP-XopL and GFP-$XopL_{K191A}$ at 1 and 2 dpi using an anti-GFP antibody. Ponceau Staining (PS) served as a loading control. The experiment was repeated three times by two different people with similar results.
(K) Mutation of Lysin 191 does not abolish poly-ubiquitination of XopL and association with NBR1. GFP-XopL and GFP-$XopL_{K191A}$ were transiently expressed in *N. benthamiana*. Samples were taken 48 hpi, and total proteins (Input) were subjected to immunoprecipitation (IP) with GFP-Trap beads, followed by immunoblot analysis of the precipitates using either anti-GFP, anti-ubiquitin and anti-NBR1 antibodies. GFP served as a control. The experiment was repeated three times with similar results.

XopL interacts with the autophagy component SH3P2 and degrades it via the proteasome to dampen autophagy

Previously, XopL was characterized as a novel class of E3 ligases capable of suppressing plant defense responses. However, its plant target(s) remained unknown (41). To analyze whether XopL directly targets autophagy components to act as an autophagy suppressor, we carried out a yeast-two hybrid (Y2H) screen using a cDNA library from tobacco (*Nicotiana tabacum*). Our previous interactions studies indicate that the tobacco cDNA library is sufficient to identify host targets of *Xcv* T3Es that are conserved across different plant species, such as pepper, tomato and *A. thaliana* (38, 49, 50). One cDNA identified in the Y2H screening for XopL interacting

proteins encoded a homologue of *A. thaliana* SH3P2, with an identity of 74 % (Fig S11A). Homologues are also present in *Nicotiana benthamiana* (NbSH3P2a and NbSH3P2b, 98% identity) and tomato (SlSH3P2, 96% to NtSH3P2) (Fig S11A, B). Direct interaction assays in yeast revealed that XopL is able to interact with SH3P2 from *N. tabacum* and *N. benthamiana* (Fig. 4A and Fig. S11C). SH3P2 from *A. thaliana* was previously identified as a novel autophagy component that interacts with ATG8 isoforms and binds to phosphatidylinositol 3-phosphate (PI3P) to regulate autophagosome formation, having also a potential role in late events of autophagy (51, 52). SH3P2 was also found to play a role in the recognition of ubiquitinated membrane proteins, and in targeting them to the endosomal sorting complexes required for transport (ESCRT) machinery (53). We next sought to determine whether the interaction between XopL and SH3P2 occurs *in planta*. Due to expression problems of tobacco SH3P2 and also due to their high identity, we conducted further interaction studies with *At*SH3P2. Using bimolecular fluorescence complementation and in *vivo* co-immunoprecipitation (co-IP), we found that XopL and *At*SH3P2 interact in the plant cell, in punctate structures resembling autophagosomes (Fig. 4B and C; Supp Video 1). Additional *in vitro* co-IP data, using *E. coli* produced recombinant MBP-XopL and GST-*At*SH3P2, suggests that XopL and SH3P2 might directly interact with each other (Fig. 4D). Given the fact that SH3P2 from *A. thaliana* interacts with ATG8 and XopL localizes in puncta within plant cells (54), we assessed whether XopL co-localizes with autophagosomes *in planta*. We were able to identify that transient expression of GFP-XopL in *N. benthamiana* with the autophagosome markers RFP epitope tagged ATG8G, ATG8E and SH3P2 resulted in strong co-localization (Fig. 4E). This further supports the idea that XopL is functioning in the autophagy pathway by associating with these components *in planta*.

Our results so far suggest that XopL might manipulate autophagy by interacting with the autophagy component AtSH3P2. Previous research on AtSH3P2 revealed that RNAi-mediated downregulation of AtSH3P2 affects the autophagy pathway (51). Since XopL possesses E3 ligase activity, we next sought to investigate whether XopL might destabilize SH3P2 and thereby block autophagic degradation. Indeed, *in planta* transient co-expression of XopL (tagged either with GFP or HA) and AtSH3P2-GFP resulted in reduced SH3P2 protein abundance in *N. benthamiana* (Fig. 4F). Degradation of AtSH3P2 by XopL was dependent on a functional proteasome, as chemical inhibition of the proteasome with MG132 partially restored AtSH3P2-GFP protein levels (Fig. 4G). To assess whether this was directly mediated by XopL and its E3 ligase activity, we performed an *in vitro* ubiquitination assay. In the presence of all required components of the E1-E2-E3 system, we observed that GST-XopL ubiquitinated MBP-AtSH3P2, which is indicated by a laddering pattern, leading to larger sized molecular species of MBP-AtSH3P2, when probed with the anti-MBP antibody (Fig. 4H). These results indicate that the E3 ligase activity of XopL might be crucial in the SH3P2-dependent modulation of host autophagy. To address this, we employed the XopL ΔE3 mutant, lacking E3 ligase activity (41, 54). Transient co-expression of XopL ΔE3 together with SH3P2 revealed that XopL requires its E3 ligase activity to trigger the degradation of AtSH3P2 in *N. benthamiana* (Fig. 4I). This was not due to an altered localization of XopL ΔE3, as it still co-localizes with AtSH3P2 upon transient expression in *N. benthamiana* (Fig. S12). As a consequence of not being able to degrade SH3P2 *in planta*, XopL ΔE3 did not lead to a suppression of autophagy responses in the quantitative luciferase autophagy assay and increase in ATG8 protein levels (Fig. 4J and K). Immunoblot analysis also revealed that XopL ΔE3 is more unstable compared to XopL WT and also degraded by autophagy, as it is not able to block autophagy (Fig S13). Taken together, our findings support the notion that the E3 ligase activity of XopL as well as its ability to directly ubiquitinate and degrade AtSH3P2 promote suppression of autophagy.

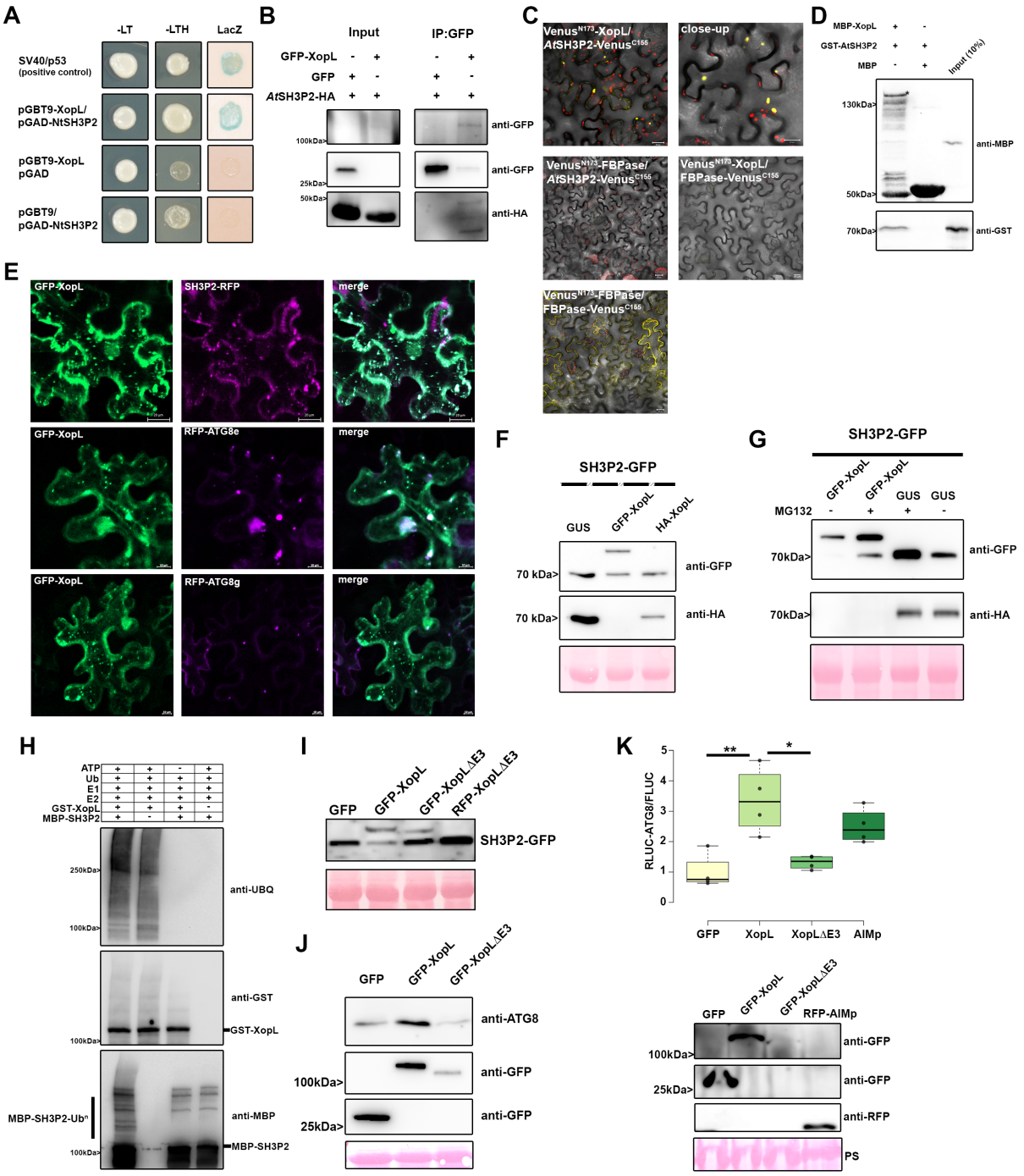

Figure 4: XopL interacts with SH3P2 and mediates its proteasome degradation via its E3 ligase activity to block autophagy

(A) Interaction of XopL with SH3P2 in yeast two-hybrid assays. XopL fused to the GAL4 DNA-binding domain was expressed in combination with SH3P2 fused to the GAL4 activation domain (AD) in yeast strain Y190. Cells were grown on selective media before a LacZ filter assay was performed. pSV40/p53 served as positive control, while the empty AD or BD vector served as negative control. NtSH3P2 = *Nicotiana tabacum* SH3P2. –LT = yeast growth on medium without Leu and Trp, –HLT = yeast growth on medium lacking His, Leu, and Trp, indicating expression of the HIS3 reporter gene. LacZ, activity of the lacZ reporter gene.

(B) Coimmunoprecipitation of GFP-XopL with AtSH3P2-HA. GFP-XopL or GFP were transiently coexpressed in leaves of *N. benthamiana* using agroinfiltration with AtSH3P2-HA. After 48 h, total proteins (Input) were subjected to immunoprecipitation (IP) with GFP-Trap

beads, followed by immunoblot analysis using either anti-GFP or anti-HA antibodies. AtSH3P2 = *Arabidopsis thaliana* SH3P2. Two repetitions with similar results have been conducted.

(C) Visualization of protein interactions *in planta* by the bimolecular fluorescence complementation assay. Yellow fluorescent protein (YFP) confocal microscopy images show *Nicotiana benthamiana* leaf epidermal cells transiently expressing $Venus^{N173}$-XopL in combination with AtSH3P2-$Venus^{C155}$. A positive control showing the dimerization of fructose-1,6-bisphosphatase (FBPase) within the cytosol. The combination of $Venus^{N173}$-XopL with FBPase-$Venus^{C155}$ or $Venus^{N173}$-FBPase with AtSH3P2-$Venus^{C155}$ do not induce YFP fluorescenc and serve as negative controls. Bars = 20 µm. AtSH3P2 = *Arabidopsis thaliana* SH3P2. The experiment has been repeated twice with similar results.

(D) *In vitro* pull-down assay showing physical interaction of XopL with AtSH3P2. MBP-XopL and GST-AtSH3P2 were expressed in E. coli. Pull down was performed using amylose resin. Proteins were detected in an immunoblot using antibodies as indicated.

(E) Colocalization analysis of GFP-XopL with SH3P2-RFP, RFP-ATG8e and RFP-ATG8g in *N. benthamiana* leaves. Imaging was performed 2 d after transient expression and images represent single confocal planes from abaxial epidermal cells (bars = 20 µm and 10 µm, lower panel). The experiment was repeated twice with similar results.

(E) Total proteins were extracted 48 hpi with *A. tumefaciens* harboring the respective GFP-XopL, HA-XopL and SH3P2-GFP expression constructs. SH3P2-GFP protein levels (lower band) were detected using an anti-GFP antibody. Expression of the XopL was verified using an anti-HA or anti-GFP antibody. Expression of GUS-HA served as a control. Ponceau S staining serves as a loading control. The experiment was repeated three times with similar results.

(F) SH3P2-GFP was transiently coexpressed together with GUS-HA and GFP-XopL in *N. benthamiana* using agroinfiltration. At 42 hpi, 200 mM MG132 was infiltrated into *A. tumefaciens*-inoculated leaves, and leaf material was collected 48 hpi. Expression of SH3P2-GFP (lower band) and GFP-XopL (upper band) was detected using an anti-GFP antibody. GUS-HA expression was confirmed with an anti-HA antibody. Ponceau S staining serves as a loading control. The experiment was repeated three times with similar results.

(G) *In vitro* ubiquitination assay reveals ubiquitination of SH3P2 by XopL. GST-XopL, and MBP-SH3P2 were tested using the Arabidopsis His-AtUBA1 and His-AtUBC8. Lanes 2 to 4 are negative controls. Proteins were separated by SDS-PAGE and detected by immunoblotting using the indicated antibodies. The experiment was repeated twice with similar results.

(H) SH3P2-GFP was transiently coexpressed together with GFP, GFP-XopL, GFP-XopL ΔE3 and RFP-XopL ΔE3 in *N. benthamiana* using agroinfiltration. GFP protein levels were detected with an anti-GFP antibody. Ponceau S staining serves as a loading control. The experiment was repeated three times with similar results.

(I) Immunoblot analysis of ATG8 protein levels in *N. benthamiana* plants transiently expressing GFP-XopL, GFP-XopL ΔE3 or GFP control at 2dpi. Expression of binary constructs was verified with an anti-GFP antibody. Ponceau Staining (PS) served as a loading control. The experiment was repeated twice with similar results.

(J) RLUC-ATG8a constructs were coexpressed with internal control FLUC in *N. benthamiana*. GFP-XopL, GFP-XopL ΔE3 or GFP control were co-infiltrated together with RLUC/FLUC mixture. *Renilla* and *Firefly* luciferase activities were simultaneously measured in leaf extracts at 48 hpi using the dual-luciferase system. Values represent the mean ratio of RLUC-ATG8a and FLUC activities and error bars show SD (n=4). Statistical significance (* $P < 0.5$, ** $P < 0.01$) was revealed by Student's *t*-test. The experiment was repeated 3 times by 2 different people with similar results. Expression of proteins was verified with indicated antibodies.

SH3P2 is required for autophagy and immunity against Xcv in N. benthamiana

Previously, downregulation of SH3P2 is *A. thaliana* has been shown to reduce autophagic activity (51). However, the role of SH3P2 is still controversial, as another study identified that SH3P2 functions in clathrin-mediated endocytosis without having any obvious effects on dark-induced autophagy (53). To shed light on the enigmatic and versatile function of SH3P2, we used virus-induced gene silencing (VIGS) in *N. benthamiana* targeting both *NbSH3P2a* and *b*. Silencing had no obvious effect on plant growth and silencing efficiency was assessed by qPCR (Fig. S14A and B). Subsequent immunoblot analysis revealed that in comparison to the pTRV2-GFP control, SH3P2 VIGS plants displayed accumulation of ATG8 protein levels, similar results to that reported by Zhuang et al. 2013 (Fig. 5A). To corroborate this finding, we transiently expressed GFP-ATG8e in control and silenced plants and monitored autophagosome formation upon AZD8055 treatment, a TOR inhibitor and autophagy activator. The number of autophagosomes increased upon AZD8055 treatment in both plants but were significantly less in SH3P2 VIGS plants when treated with ConA (Fig. 5B and C). This indicates that downregulation of SH3P2 in *N. benthamiana* impairs maturation of autophagosomes and hence autophagic degradation. Indeed, using confocal microscopy of GFP-ATG8E, we observed aberrant autophagosomal structures in VIGS SH3P2 plants that might explain why autophagy is not entirely functional anymore. These data suggest that SH3P2 might be required during later steps as autophagosome induction seems to be normal during autophagy induction with AZD8055. VIGS in *N. benthamiana roq1* plants and subsequent bacterial growth measurements with *Xcv* and *Xcv ΔxopL* revealed that pTRV2-*SH3P2* plants are more susceptible towards *Xcv* similar to pTRV2-*Joka2* plants (Fig. 5D). Essentially, reduced growth of *Xcv ΔxopL* was rescued in both SH3P2 and Joka2 silenced plants strengthening our findings that XopL suppresses both bulk and selective autophagy pathways to cause disease (Fig. 5D).

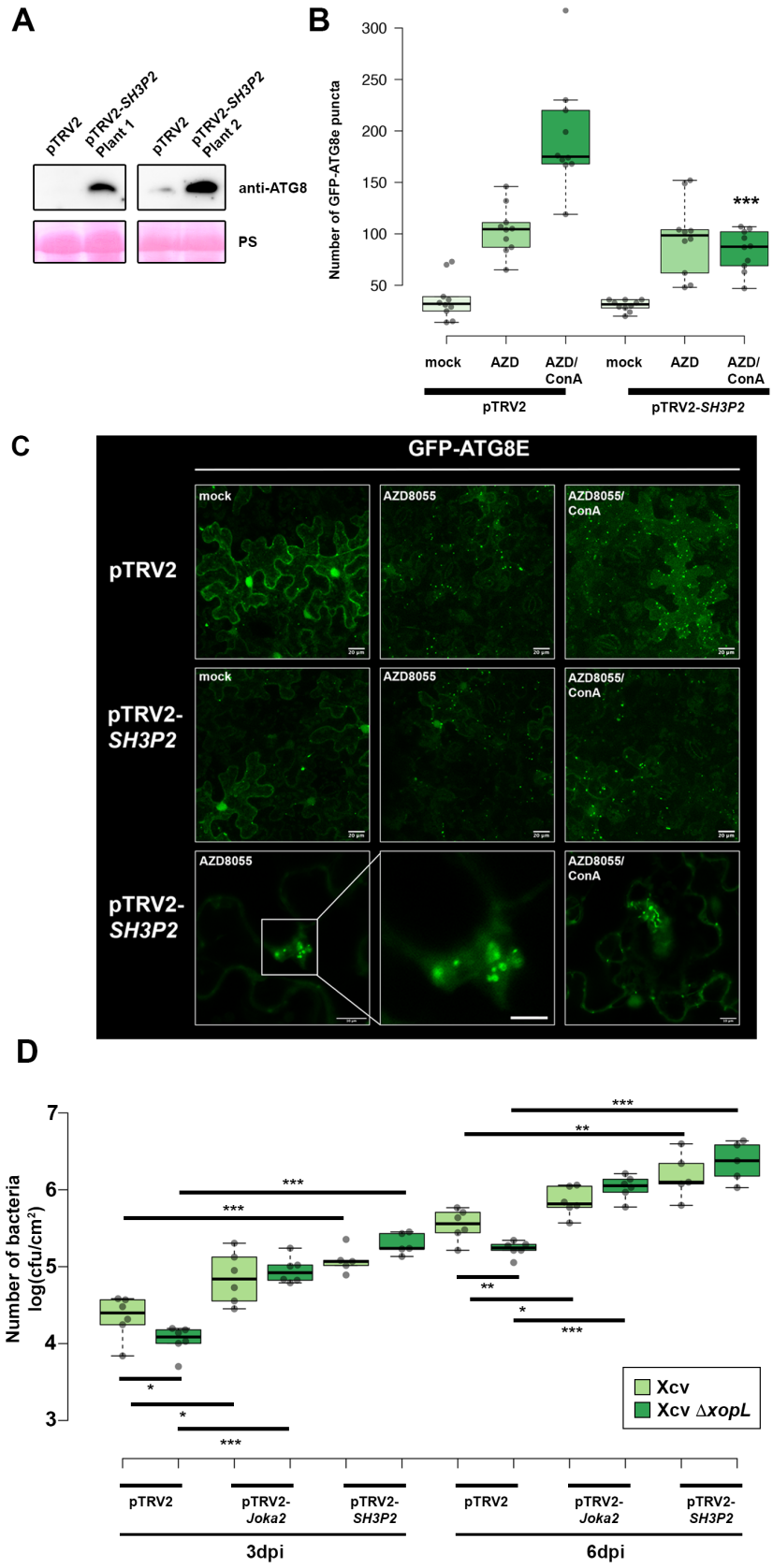

Figure 5: Silencing of SH3P2 suppresses autophagic degradation and is beneficial for *Xanthomonas* growth

(A) Immunoblot analysis of ATG8 protein levels in *N. benthamiana* pTRV2 (control) and pTRV2-*SH3P2* (*SH3P2* silencing) 2 weeks after VIGS. Ponceau Staining (PS) served as a loading control. The experiment was repeated twice with similar results.

(B) GFP-ATG8e-labeled autophagosomes were quantified from pTRV2 or pTRV2-SH3P2 plants transiently expressing GFP-ATG8e at 2dpi in the presence of autophagy inducer AZD = AZD8055 and AZD/ConA. Puncta were calculated from z-stacks of n=10 individuals using ImageJ. Statistical significance (*** $P < 0.5$) was revealed by Student's t-test comparing number of autophagosomes in AZD/ConA treatments in pTRV2 and pTRV2-*SH3P2* plants. The experiment was repeated twice with similar results.
(C) Transient expression of GFP-ATG8E in pTRV2 and pTRV2-*SH3P2* plants with indicated treatments (mock, AZD8055, AZD8055/ConA). Confocal images were taken at 1dpi. Scale bars are indicated in the figure. Square indicates area that was used for a close-up image (Bar = 5 μm).
(D) Growth of Xcv *and* Xcv *ΔxopL* strains in *roq1 N. benthamiana* plants silenced for SH3P2 and Joka2 (pTRV2-*SH3P2*, pTRV2-*Joka2*) compared to control plants (pTRV2). Leaves were dip-inoculated with a bacteria suspension at OD_{600} = 0.2 and bacteria were quantified at 3, 6 dpi. Data represent the mean SD (n = 6) and n = 5 for pTRV2-*SH3P2*. Significant differences were calculated using Student's *t-test* and are indicated by: *, $P < 0.05$; **, $P < 0.01$; ***, $P < 0.001$ The experiment was repeated more than more than two times with similar trends.

Discussion

The role of autophagy in host-microbe interactions has remained enigmatic and puzzling. Previous studies have reported that autophagy is modulated during host-bacteria interactions and that bacterial effectors actively regulate this process (22, 55). Across kingdoms, autophagy has both pro- and anti-bacterial activities (12, 25). In animals and also plant-virus interactions, the role of anti-microbial autophagy has been attributed mostly to xenophagy, the autophagic degradation of pathogens or pathogenic molecules which can be counteracted by microbial effectors (13, 56). In contrast to animal pathogenic bacteria, plant gram negative pathogenic bacteria reside in the apoplast without being in contact with the intracellular autophagy machinery. The only bacterial components present inside the cell are T3Es that have been shown to actively modulate autophagy responses (18, 26). However, little is known about how they mechanistically regulate autophagy and whether they are potential targets of xenophagy.
Here, by studying *Xanthomonas*-host interactions, we revealed a complex-layered regulatory role of autophagy in plant immunity. We demonstrate that anti-bacterial autophagy is activated during Xanthomonas infection by targeting the bacterial effector XopL and utilizing NBR1/Joka2-triggered selective autophagy. However, XopL might act as a trap to access the autophagy machinery and suppress it for its own benefit. Indeed, we here unveil that E3 ligase XopL associates with and ubiquitinates the autophagy component SH3P2 to degrade it by the proteasome. This in turn, dampens autophagy, hampering the delivery of cargos, including XopL, into the lytic vacuole. Both the block of autophagy and also rescue of XopL is beneficial for the bacterium as anti-bacterial autophagy is eliminated and pathogenicity restored (Fig. S15).

Autophagy in host-immune interactions

Over the recent years, autophagy has emerged as one of the main targets of animal and plant pathogens, not only due to its role in maintaining a functional environment but also due to its participation in immune responses (9, 57). In animals, several pathogenic bacteria have been identified to modulate the autophagy pathway to their own benefit (12). Many intracellular animal pathogenic bacteria can be eliminated by autophagy, while others (such as *Shigella*, *Yersinia* and *Listeria*), are able to exploit autophagy to increase their pathogenicity (12). In plants, several studies have highlighted that pathogens manipulate the autophagy pathway (58). More specifically, the plant pathogenic bacterium *Pseudomonas syringae* pv. *tomato* (*Pst*) has been shown to utilize effectors to modulate autophagic degradation (18, 26). However, autophagy seems to display contrasting pro-and antibacterial effects. On the one hand,

autophagy is beneficial for the virulence of *Pst* while on the other hand, NBR1-dependent autophagy restricts pathogen growth (18). With *Xcv,* we have identified another plant pathogenic bacterium that modulates autophagy, similar to *Pst*, in an effector-dependent manner. Although, both pathogens have the same habitat and hemi-biotrophic lifestyle, they act in different ways on the autophagy pathway. For *Xcv* inhibition of the autophagy pathway is crucial to maintain pathogenicity while *Pst* activates it for its own benefit. Previously, it has been reasoned that autophagy activation might be essential to maintain plant viability and lifespan (19). However, autophagy may not be required for this during *Xcv* infection, as it has been shown that T3Es XopD and XopJ are able to prolong the biotrophic phase by other mechanisms (38, 59). As such, autophagy is dispensable for the virulence of *Xcv* and actively blocked to prevent xenophagy of effector(s), which we here term "effectorphagy". *Xanthomonas* is able to block effectorphagy by targeting SH3P2 for degradation. SH3P2 was first identified as a novel autophagy component, stimulating autophagosome formation during nitrogen starvation and BTH-triggered immune responses (51). Later studies also showed that SH3P2 plays a key role in membrane tubulation during cell plate formation (60) and clathrin-mediated endosomal sorting and degradation, with no effect in dark-induced autophagy (53). Our findings that loss of SH3P2 from *N. benthamiana* impairs autophagy and promotes pathogenicity sheds further light on its diverse functions. However, the effects of XopL on SH3P2 and increasing virulence of *Xcv* might not only be attributed to its function in autophagy. Because endocytic trafficking also plays a major role in plant immunity (61), it is likely that XopL has a function beyond autophagy to impair plant defense mechanisms. This is also supported by the fact that XopL is able to reduce PTI responses (41), which is not due its function in autophagy, as autophagy deficiency has no impact on PTI responses (62).

In summary, the anti- and pro-bacterial effects of autophagy seem to be very complex. In some cases, both, anti- and pro-bacterial effects seem to operate during host-bacteria interactions. Specifically, recent findings indicate that *Pst* seems to possess T3Es that are able to impair autophagy (26). This suggests that multiple autophagy pathways with opposing effects might operate in parallel. This apparent contradiction is supported by findings of animal pathogenic bacteria: *Salmonella* has been shown to be degraded by p62-mediated selective autophagy but at the very same time requires the autophagy pathway to replicate in HeLa cells (63, 64). These findings add a certain complexity to the role of autophagy in host-microbe interactions that might be explained by cell-type specific responses or operation of various selective autophagy pathways that might be specifically targeted by the pathogens.

Role of xenophagy in immunity

One of the best studied selective autophagy receptors across kingdoms is NBR1/p62 that plays a central role in xenophagy and degradation of protein aggregates (35, 67). Its role in plant immune responses has been shown by the involvement of NBR/Joka2-mediated selective autophagy in restricting pathogen growth or disease progression during *P. infestans* or *Pst* infection (16, 18). In animals, p62, the counterpart of plant NBR1, functions to mediate xenophagy, which has been also described for NBR1 in plants in a plant-virus infection context but not for other plant pathogens (19, 20). Our analysis provides the first evidence that similar to viral proteins, bacterial effectors may also constitute a target of NBR1-mediated selective autophagy. We found that XopL is targeted by NBR1/Joka2 for autophagic degradation shedding light on the function of NBR1/Joka2 to restrict pathogen growth. We hypothesize that XopL might have been used as a bait to access the autophagy pathway in order to boost virulence of *Xcv* by attenuating autophagic degradation. Initially, targeted by NBR1/Joka2-dependent autophagy, a sub-proportion of XopL is “sacrificed” and ends up in the vacuole for degradation. However, as XopL is able to associate with and degrade the autophagy component SH3P2, it partially escapes its own degradation and blocks autophagy. Although, XopL is able to suppress autophagy, its activity to block the pathway is still less than the recently discovered AIMp, which acts as a potent autophagy inhibitor (34). This also explains why XopL is still

degraded. To date, it has not been reported that bacterial effectors in animals and plants are removed by selective autophagy as an anti-microbial response. Although, a recent study by Pandey et al. 2020 identified that an oomycete effector from *P. infestans* is degraded by autophagy, its mode of action and consequences remain unknown (34). Interestingly, the *Salmonella* effector SseL, which inhibits selective autophagy to abolish p62-dependent degradation of *Salmonella*, was also found to interact with p62 (68). This might suggest the possibility that SseL might also have been an autophagy target before it acquired its function to block this pathway via its deubiquitinase activity (68). We hypothesize that NBR1/p62 might have evolved to have a function in anti-bacterial autophagy by triggering xenophagy of bacterial molecules as an alternative strategy to degrade entire intracellular bacteria. This may have happened for the function of NBR1 in plants, as fungal and oomycete pathogens as well as gram negative bacteria reside in the extracellular space. Animal pathogens also occupy the extracellular space, before entering the host cell. In the case of *Salmonella*, it first needs to inject bacterial effectors via its SPI-1 T3SS to establish internalization and its replication niche (69). It is therefore tempting to speculate that these effectors may be targeted by selective autophagy mechanisms as an early defense mechanism of the immune system. Similar to XopL, several of the SPI1 T3Es, e.g., SopA as well as SopE can mimic E3 ligases and/or are ubiquitinated in the host cell (70), making them ideal targets for NBR1/p62-mediated selective autophagy. Indeed, SopA and SopE have been reported to be degraded through the proteasome (71, 72). A possible degradation by autophagy was not investigated in these studies. Our results also suggest that XopL is targeted by a host E3 ligase for degradation as the XopL variant lacking E3 ligase activity is still ubiquitinated *in planta* and degraded by autophagy. Several E3 ligases have been implicated in plant-microbe interactions, which opens up the possibility that they may target microbial proteins (73).

Although plant pathogenic bacteria possess T3Es that are implicated in the host ubiquitin system, to date there is no evidence that they might be ubiquitinated in the host. In addition, we identified that XopL undergoes self-ubiquitination, which has not been reported for animal and plant pathogenic bacterial effectors. This might constitute a novel mechanism how these effectors exploit degradation system. To date, autoubiquitination of E3 ligases has been assigned as a mechanism of self-regulation through which their activity is controlled (54). In the case of bacterial T3Es that mimic E3 ligases, it might be a strategy to trick degradation systems. Given the fact that XopL belongs to the IpaH E3 ligase family of effectors that are widely conserved among animal and plant pathogens (74), we envision that similar mechanisms might act across kingdoms. Indeed, T3E IpaH1.4 from *Shigella* blocks autophagy through a different mechanism (75). Future research on the IpaH E3 ligase family of effectors might reveal whether they possess self-ubiquitination activity and utilize this to trick the host immune system or to modulate their activity within the host.

Taken together, we provide a primary example of an effector with self-ubiquitination activity which makes it a target of selective autophagy. We provide evidence that by self-ubiquitination, XopL first presents itself as a target of autophagy and then degrades the autophagy component SH3P2, in order to block the autophagy machinery. Together, our observations uncover a novel mechanism how a bacterial effector modifies itself to hijack the host autophagy system.

Material and Methods

Plant Material and Growth Conditions

Wild-type plants were *Arabidopsis thaliana* ecotype Columbia (Col-0) and *Nicotiana benthamiana. Arabidopsis* plants were grown on soil under short-day conditions (8/16-h light/dark cycles) in a growth chamber or for maintenance and crossings under long-day conditions (16/8-h light/ dark cycles) in a growth room with light intensity of 150 µE, 21°C,

and 70% relative humidity, respectively. *N. benthamiana* plants were grown under long day conditions 16/8-h light/dark cycles, 21°C, and 70% relative humidity.

Bacterial growth conditions

Agrobacterium tumefaciens, Agrobacteria strain C58C1 was grown in LB Hi-Salt (10g/L sodium chloride, 10g/L tryptone, 5g/L yeast extract) with 100 µg mL−1 rifampicin at 28 °C. The cultures supplemented with the appropriate antibiotics for those harbouring plasmids. Xcv strain 85-10 was grown in NYG media (0.5% peptone, 0.3% yeast extract, 2% glycerol) with 100 µg mL−1 rifampicin at 28 °C.

Construction of Xcv Δ*xopL* and Δ*xopQ* null mutants

To construct Xcv 85-10 *xopL* and *xopQ* deletion mutants, the 1.7-kb upstream and downstream regions of the xopL or xopQ gene were PCR amplified using Xcv 85-10 genomic DNA as template and cloned into pLVC18 linearized with EcoRI (New England Biolabs) using Gibson assembly. The plasmid was introduced into Xcv 85-10 by triparental mating. Xcv transconjugants were analysed by PCR to confirm that homologous recombination occurred at the xopL or XopQ locus.

Constructs for Xcv Δ*xopL* complementation analysis

To construct xopL gene with 0.3-kb promoter region in broad host range vector, 0.3-kb promoter-xopL gene was PCR amplified using Xcv 85-10 genomic DNA as template and cloned into pBBR1MCS-2 (76) linearized with EcoRV (New England Biolabs) using Gibson assembly. The plasmid was introduced into Xcv 85-10 Δ*xopL* by triparental mating.

Bacterial infection

Xcv carrying a deletion mutation of XopQ (Xcv *ΔxopQ*), or of HrcN (Xcv Δ*hrcN*), or of both XopQ and XopL (Xcv *ΔxopQ ΔxopL*) were used to infect wild-type *N. benthamiana*. Xcv were grown overnight in NYG with appropriate antibiotics at 28°C with shaking. Bacteria were diluted to OD_{600} = 0.2 for dual-luciferase assays, immunoblot analysis of NBR1, ATG8 or confocal microscopy of autophagosomal structures. For in planta growth curves using syringe infiltration, Xcv strains were inoculated at OD_{600} = 0.0004, and for dip-inoculation OD_{600} = 0.2 was used.

Tomato growth condition and bacterial growth assay

Tomato (*Solanum lycopersicum*) cv. VF36 was grown in greenhouse (22-28 °C, 50-70 % RH, 16-h light). For bacterial growth assays, leaflets were dipped in a 2 x 10^8 CFU/mL suspension of Xcv 85-10 strains in 10mM MgCl2 with 0.025% (v/v) silwet L-77 (Helena Chemical Company) for 30 sec. Plants were then placed in plastic chambers at high humidity (>95%) for 24 h. For each strain analyzed, four leaf discs (0.5 cm^2) per treatment per timepoint were ground in 10 mM $MgCl_2$ and diluted and spotted onto NYGA plates in triplicate to determine bacterial load. Three biological replicates (i.e., three plants) were used, and the experiment was repeated at least three times.

Plasmid construction

For transient expression experiments, the coding region of XopL, AtSH3P2 or SlJoka2 were cloned into pENTR/D-TOPO and subsequently recombined into pUBN-DEST-GFP or RFP (77), pGWB614/5 (78), pMAlc2, pDEST15. The RFP-ATG8E/G, GFP-ATG8e, RFP-NBR1, RLUC-ATG8, RLUC-NBR1, XopD-GFP, XopJ-GFP, pTRV2-Joka2, pTRV2-ATG7 constructs were described previously (18, 38). All binary plasmids were transformed into Agrobacterium tumefaciens strain C58C1 and infiltration of *N. benthamiana* was done at the

four-to six-leaf stage. Stable Arabidopsis transformation was performed using the floral dip method (79).

Transient Expression in *N. benthamiana* by Agrobacterium-Mediated Leaf Infiltration

Agrobacterium strains harboring the indicated plasmids were grown overnight in liquid LB media at 28°C with appropriate antibiotics and harvested by centrifugation at 4000g for 15 min. Bacterial pellets were washed once in double-distilled water, resuspended in infiltration buffer (10 mM MES, pH5.7, 10 mM $MgCl_2$, and 150 µM acetosyringone). The OD_{600} = 0.2 of each culture was adjusted such that approximately equal numbers of bacteria from cultures expressing different transgenes were mixed and infiltrated into *N. benthamiana* leaves using a needleless syringe.

Confocal Microscopy

Live-cell images were acquired from abaxial leaf epidermal cells using a Zeiss LSM780 and LSM880 microscope. Excitation/emission parameters for GFP and RFP were 488 nm/490 to 552 nm and 561 nm/569 to 652 nm, respectively, and sequential scanning mode was used for colocalization of both fluorophores. Confocal images with ImageJ (version 2.00) software. Quantification of ATG8a-labeled autophagosomal structures was done on z-stacks that were converted to eight-bit grayscale and then counted for ATG8 puncta either manually or by the Particle Analyzer function of ImageJ.

FRET-FLIM measurement

FRET-FLIM was performed on SP8 confocal laser scanning microscope (CLSM) (Leica Microsystems GMBH) with LAS AF and SymPhoTime 64 software using a 63x/1.20 water immersion objective. FLIM measurements were performed with a 470 nm pulsed laser (LDH-P-C-470) with 40 MHz repetition rate and a reduced speed yielding, with an image resolution of 256x256, a pixel dwell time of ~10 µs. Max count rate was set to ~15000 cps. Measurements were stopped, when the brightest pixel had a photon count of 1000. The corresponding emission was detected with a Leica HyD SMD detector from 500 nm to 530 nm by time-correlated single-photon counting using a Timeharp260 module (PicoQuant, Berlin). The calculation of GFP lifetime was performed by iterative reconvolution, i.e. the instrument response function was convolved with exponential test functions to minimize the error with regard to the original TCSPC histograms in an iterative process. For measurements of GFP-JOKA2 protein aggregates, ROIs where drawn manually on SymphoTime64 software around the aggregates to analyze GFP lifetime in these structures.

Immunoprecipitation

GFP pull-down assays were performed as previously described (18) with minor modifications. Approximately 2 g of leaf material was ground to a fine powder in liquid nitrogen and homogenized in 4 mL of extraction buffer (25 mM Tris-HCl, pH 7.5, 150 mM NaCl, 10%glycerol, 1 mM DTT, 1 mM EDTA, 1% [v/v] protease inhibitor cocktail, and 0.5% TritonX). Insoluble debris was pelleted by centrifugation for 20 min with 4000 rpm at 4°C. Immunoprecipitation was performed by adding 30 mL of GFP-Trap coupled to agarose beads (ChromoTek) and samples were incubated for 2 h at 4°C with continual rotation. Beads were subsequently washed five times with Tris-buffered saline containing 0.5% Triton X, and immunoprecipitates were eluted with 30 µL of 2x SDS loading buffer at 70°C for 10 min. Pulldown of ubiquitinated proteins according to manufacturer's instructions (NanoTag Biotechnologies).

***In vitro* pull-down**

Recombinant proteins from *Escherichia coli* lysates were immobilized on amylose resins (New England Biolabs), incubated for 1 h at 4 °C with purified GST-SH3P2, eluted, and analyzed by immunoblotting using either anti-GST antibody (Sigma) or anti- MBP antibody (NEB).

In vitro ubiquitination assay

Recombinant proteins were expressed in *E. coli* BL21(DE3) and purified by affinity chromatography using amylose resin (New England Biolabs). Recombinant His-UBA1 and His-UBC8 were purified using Ni-Ted resin (Macherey-Nagel). Purified proteins were used for *in vitro* ubiquitination assays. Each reaction of 30 mL final volume contained 25 mM Tris-HCl, pH 7.5, 5 mM MgCl2, 50 mM KCl, 2 mM ATP, 0.6 mM DTT, 2 µg ubiquitin, 200 ng E1 His-*At*UBA1, 1.2 µg E2 His-*At*UBC8, 2 µg of E3s, and 0.3 µg of MBP-*At*SH3P2. Samples were incubated for 1h at 30°C and reaction was stopped by adding SDS loading buffer and incubated for 10 min at 68°C. Samples were separated by SDS-PAGE electrophoresis using 4–15% Mini-PROTEAN® TGX™ Precast Protein Gels (BioRad) followed by detection of ubiquitinated substrate by immunoblotting using anti-MBP (New England Biolabs), anti-GST and anti-ubiquitin (Santa Cruz Biotechnology) antibodies.

Immunoblot analysis

Proteins were extracted in 100 mM Tris (pH 7.5) containing 2% SDS, boiled for 10min in SDS loading buffer, and cleared by centrifugation. The protein extracts were then separated by SDS-PAGE, transferred to PVDF membranes (Biorad), blocked with5% skimmed milk in PBS, and incubated with primary antibodies anti-NBR1 (Agrisera), anti-ATG8 (Agrisera), anti-ubiquitin (Agrisera), anti-GFP (SantaCruz), anti-RFP (Chromotek), anti-HA (Sigma Aldrich) primary antibodies using 1:2000 dilutions in PBS containing 0.1% Tween 20. This was followed by incubation with horseradish peroxidase-conjugated secondary antibodies diluted 1:10,000 in PBS containing 0.1% Tween 20. The immunoreaction was developed using an ECL Prime Kit (GE Healthcare) and detected with Amersham Imager 680 blot and gel imager.

Dual Luciferase Assay

The dual luciferase reporter assay was performed according to the manufacturer's instructions (Dual-Luciferase Reporter Assay System; Promega) with slight modifications. Briefly, four leaf discs were homogenized in 200 µL lysis buffer and cleared by centrifugation. For detection and measurement of the Fireflyluciferaseactivity,40 µL of the luciferase assay reagent was added to 5 µL of plant extracts. To measure *Renilla* luciferase activity, 40 µL of the Stop and Glo reagent was added to the mixture. The measurement was performed in a plate reader.

Virus-induced gene silencing

VIGS was performed as described previously (38). In brief, fragment of SH3P2 was amplified by PCR and cloned into pTRV2-Gateway using the Gateway recombination system. Primer sequences are listed in Supplemental Table 1 online. The resulting plasmids were transformed into *Agrobacterium tumefaciens* C58C1. A lower leaf of a 2-week-old *N. benthamiana* plant (four-leaf stage) was co-infiltrated with a mixture of Agrobacteria carrying either pTRV1, a binary vector expressing TRV subgenomic RNA1 under control of the cauliflower mosaic virus 35S promoter, or pTRV2 expressing TRV subgenomic RNA2 and containing the target sequence. Silenced plants were analyzed 14 d after infiltration.

RNA extraction and RT-qPCR

RNA was extracted from 4 leaf discs according to manufacturer instructions using the GeneMATRIX Universal RNA Purification Kit (Roboklon) with on-column DNase I digestion. RNA integrity was checked by loading on 1% agarose gel and separating by electrophoresis. RNA concentrations were measured using Nanodrop 2000 (Thermo Fisher), and equal amounts

of RNA were used for cDNA synthesis. cDNA synthesis was performed using LunaScript™ RT SuperMix Kit (New England Biolabs) and in a standard thermocycler according to manufacturer instructions. Gene expression was measured by qPCR using MESA BLUE qPCR MasterMix Plus for SYBR® Assay No ROX (Eurogentec) and cycle quantification by Biorad CFX system.

NanoLC-MS/MS analysis and data processing

Proteins were purified on an NuPAGE 12% gel (Invitrogen) and Coomassie-stained gel pieces were digested in gel with trypsin as described previously (80) with a small modification: chloroacetamide was used instead of iodoacetamide for carbamidomethylation of cysteine residues to prevent formation of lysine modifications isobaric to two glycine residues left on ubiquitinylated lysine after tryptic digestion. After desalting using C18 Stage tips peptide mixtures were run on an Easy-nLC 1200 system coupled to a Q Exactive HF-X mass spectrometer (both Thermo Fisher Scientific) as described elsewhere (81) with slight modifications: the peptide mixtures were separated using a 87 minute segmented gradient from 10-33-50-90% of HPLC solvent B (80% acetonitrile in 0.1% formic acid) in HPLC solvent A (0.1% formic acid) at a flow rate of 200 nl/min. The seven most intense precursor ions were sequentially fragmented in each scan cycle using higher energy collisional dissociation (HCD) fragmentation. In all measurements, sequenced precursor masses were excluded from further selection for 30 s. The target values were 105 charges for MS/MS fragmentation and 3x106 charges for the MS scan.

Acquired MS spectra were processed with MaxQuant software package version 1.5.2.8 with integrated Andromeda search engine. Database search was performed against a *Nicotiana benthamiana* database containing 74,802 protein entries, the sequences of XopL from *Xanthomonas campestris* pv. *vesicatoria*, and 285 commonly observed contaminants. Endoprotease trypsin was defined as protease with a maximum of two missed cleavages. Oxidation of methionine, phosphorylation of serine, threonine and tyrosine, GlyGly dipetide on lysine residues, and N-terminal acetylation were specified as variable modifications. Carbamidomethylation on cysteine was set as fixed modification. Initial maximum allowed mass tolerance was set to 4.5 parts per million (ppm) for precursor ions and 20 ppm for fragment ions. Peptide, protein and modification site identifications were reported at a false discovery rate (FDR) of 0.01, estimated by the target-decoy approach (Elias and Gygi). The iBAQ (Intensity Based Absolute Quantification) and LFQ (Label-Free Quantification) algorithms were enabled, as was the "match between runs" option (82).

Drug treatments

For the analysis of protein stability 200 mM MG132 or 1% EtOH was infiltrated to plants transiently expressing binary constructs 2dpi. 6 hours later leaf material was harvested. were analysed under the CLSM. Concanamycin A treatment was performed by syringe infiltration of mature leaves with 0.5 µM ConA for 6-8 h prior confocal analysis or immunoblot analysis. AZD8055 (15 µM) was done for 6-8 hours prior confocal microscopy.

Phylogenetic Analysis

An alignment between SH3P2 proteins was generated using ClustalW wand the tree was generated using the neighbor-joining method.

Data Analysis and Presentation

Data are presented as mean SD. Statistical significance was analysed by Student's t test (*P < 0.05, **P < 0.01, and P*** < 0.001). The number of biological replicates (n) is given in the figure legends. Statistical analyses and graphical presentation of data were made in R and RStudio (Version 1.2.5033). Boxplots were prepared using the ggplot2 package.

Author contributions

J.-X.L, S.Ü., M.R., D.S., G.L., A.R.G., J.-G.K., M.F.-W. performed the experiments. A.E.A.M., M.F.W., B.M., A.H., T.O.B., M.B.M., F.B., D.H., and S.Ü. analysed the data. P.P. and T.O.B. provided unpublished material. S.Ü. planned the project and wrote the article with input from all authors.

Acknowledgements

We thank Ingrid Schießl for the initial Y2H screen with XopL. We also thank Tom Denyer for critical reading of the manuscript and "brainstorming" sessions to find a suitable title. We thank Johannes Stuttmann for the *roq1 N. benthamiana* seeds. We thank Silke Wahl and Irina Droste-Borel for technical support for the proteomics assay. This work was supported by an Emmy Noether Fellowship GZ: UE188/2-1 from the Deutsche Forschungsgemeinschaft (DFG; to SÜ), and through the collaborative research council 1101 (SFB1101; to GL). A.E.A.M. was supported by EU Horizon 2020 MSCA IF (799433). F.B. was supported by funds from the DFG (BO1961/5-2). D.H, was supported by grants from the Swedish research councils VR (2016-04562; 2020-05327) and FORMAS (2017-01596). T.O.B. was supported by BBSRC - Biotechnology and Biological Sciences Research Council, grant code BB/T006102/1. M.B.M. was supported by NSF IOS Grant 2026368. FORMAS (grant number 2016-01044) for A.H.

References

1. C. Pohl, I. Dikic, Cellular quality control by the ubiquitin-proteasome system and autophagy. *Science* **366**, 818-822 (2019).
2. R. S. Marshall, R. D. Vierstra, Autophagy: The Master of Bulk and Selective Recycling. *Annual review of plant biology* **69**, 173-208 (2018).
3. H. Hu, S. C. Sun, Ubiquitin signaling in immune responses. *Cell research* **26**, 457-483 (2016).
4. E. H. G. Adams, S. H. Spoel, The ubiquitin-proteasome system as a transcriptional regulator of plant immunity. *Journal of experimental botany* **69**, 4529-4537 (2018).
5. N. Germic, Z. Frangez, S. Yousefi, H. U. Simon, Regulation of the innate immune system by autophagy: neutrophils, eosinophils, mast cells, NK cells. *Cell death and differentiation* **26**, 703-714 (2019).
6. B. Levine, N. Mizushima, H. W. Virgin, Autophagy in immunity and inflammation. *Nature* **469**, 323-335 (2011).
7. Y. Yang, D. J. Klionsky, Autophagy and disease: unanswered questions. *Cell death and differentiation* **27**, 858-871 (2020).
8. S. Üstün, A. Hafrén, D. Hofius, Autophagy as a mediator of life and death in plants. *Current opinion in plant biology* **40**, 122-130 (2017).
9. A. Y. Leary, Z. Savage, Y. Tumtas, T. O. Bozkurt, Contrasting and emerging roles of autophagy in plant immunity. *Current opinion in plant biology* **52**, 46-53 (2019).
10. N. Germic, Z. Frangez, S. Yousefi, H. U. Simon, Regulation of the innate immune system by autophagy: monocytes, macrophages, dendritic cells and antigen presentation. *Cell death and differentiation* **26**, 715-727 (2019).
11. S. Mostowy, Autophagy and bacterial clearance: a not so clear picture. *Cellular microbiology* **15**, 395-402 (2013).
12. J. Huang, J. H. Brumell, Bacteria-autophagy interplay: a battle for survival. *Nature reviews. Microbiology* **12**, 101-114 (2014).
13. L. C. Gomes, I. Dikic, Autophagy in antimicrobial immunity. *Molecular cell* **54**, 224-233 (2014).

14. S. J. van Wijk *et al.*, Fluorescence-based sensors to monitor localization and functions of linear and K63-linked ubiquitin chains in cells. *Molecular cell* **47**, 797-809 (2012).
15. N. Dupont *et al.*, Shigella phagocytic vacuolar membrane remnants participate in the cellular response to pathogen invasion and are regulated by autophagy. *Cell host & microbe* **6**, 137-149 (2009).
16. Y. F. Dagdas *et al.*, An effector of the Irish potato famine pathogen antagonizes a host autophagy cargo receptor. *Elife* **5** (2016).
17. Y. F. Dagdas *et al.*, Host autophagy machinery is diverted to the pathogen interface to mediate focal defense responses against the Irish potato famine pathogen. *Elife* **7** (2018).
18. S. Üstün *et al.*, Bacteria Exploit Autophagy for Proteasome Degradation and Enhanced Virulence in Plants. *The Plant cell* **30**, 668-685 (2018).
19. A. Hafrén *et al.*, Selective autophagy limits cauliflower mosaic virus infection by NBR1-mediated targeting of viral capsid protein and particles. *Proceedings of the National Academy of Sciences of the United States of America* **114**, E2026-E2035 (2017).
20. A. Hafrén *et al.*, Turnip Mosaic Virus Counteracts Selective Autophagy of the Viral Silencing Suppressor HCpro. *Plant physiology* **176**, 649-662 (2018).
21. M. Khan, D. Seto, R. Subramaniam, D. Desveaux, Oh, the places they'll go! A survey of phytopathogen effectors and their host targets. *The Plant journal : for cell and molecular biology* **93**, 651-663 (2018).
22. G. Langin, P. Gouguet, S. Üstün, Microbial Effector Proteins - A Journey through the Proteolytic Landscape. *Trends in microbiology* **28**, 523-535 (2020).
23. M. J. Banfield, Perturbation of host ubiquitin systems by plant pathogen/pest effector proteins. *Cellular microbiology* **17**, 18-25 (2015).
24. S. Üstün *et al.*, The Proteasome Acts as a Hub for Plant Immunity and Is Targeted by Pseudomonas Type III Effectors. *Plant physiology* **172**, 1941-1958 (2016).
25. S. Üstün, D. Hofius, Anti- and pro-microbial roles of autophagy in plant-bacteria interactions. *Autophagy* **14**, 1465-1466 (2018).
26. N. K. Lal *et al.*, Phytopathogen Effectors Use Multiple Mechanisms to Manipulate Plant Autophagy. *Cell host & microbe* **28**, 558-571 e556 (2020).
27. S. Timilsina *et al.*, Xanthomonas diversity, virulence and plant-pathogen interactions. *Nature reviews. Microbiology* **18**, 415-427 (2020).
28. S. Üstün, F. Börnke, Interactions of Xanthomonas type-III effector proteins with the plant ubiquitin and ubiquitin-like pathways. *Frontiers in plant science* **5**, 736 (2014).
29. D. Buttner, Behind the lines-actions of bacterial type III effector proteins in plant cells. *FEMS microbiology reviews* **40**, 894-937 (2016).
30. Y. Yan, P. Wang, C. He, H. Shi, MeWRKY20 and its interacting and activating autophagy-related protein 8 (MeATG8) regulate plant disease resistance in cassava. *Biochemical and biophysical research communications* **494**, 20-26 (2017).
31. H. Zeng *et al.*, Molecular identification of GAPDHs in cassava highlights the antagonism of MeGAPCs and MeATG8s in plant disease resistance against cassava bacterial blight. *Plant molecular biology* **97**, 201-214 (2018).
32. N. Adlung *et al.*, Non-host Resistance Induced by the Xanthomonas Effector XopQ Is Widespread within the Genus Nicotiana and Functionally Depends on EDS1. *Frontiers in plant science* **7**, 1796 (2016).
33. A. N. Dauphinee *et al.*, Chemical Screening Pipeline for Identification of Specific Plant Autophagy Modulators. *Plant physiology* **181**, 855-866 (2019).
34. P. Pandey *et al.*, The Irish potato famine pathogen subverts host vesicle trafficking to channel starvation-induced autophagy to the pathogen interface. *bioRxiv* 10.1101/2020.03.20.000117, 2020.2003.2020.000117 (2020).

35. S. Svenning, T. Lamark, K. Krause, T. Johansen, Plant NBR1 is a selective autophagy substrate and a functional hybrid of the mammalian autophagic adapters NBR1 and p62/SQSTM1. *Autophagy* **7**, 993-1010 (2011).
36. E. A. Minina et al., Transcriptional stimulation of rate-limiting components of the autophagic pathway improves plant fitness. *Journal of experimental botany* **69**, 1415-1432 (2018).
37. J. Gantner, J. Ordon, C. Kretschmer, R. Guerois, J. Stuttmann, An EDS1-SAG101 Complex Is Essential for TNL-Mediated Immunity in Nicotiana benthamiana. *The Plant cell* **31**, 2456-2474 (2019).
38. S. Üstün, V. Bartetzko, F. Börnke, The *Xanthomonas campestris* type III effector XopJ targets the host cell proteasome to suppress salicylic-acid mediated plant defence. *PLoS pathogens* **9**, e1003427 (2013).
39. C. Lorenz, D. Buttner, Functional characterization of the type III secretion ATPase HrcN from the plant pathogen *Xanthomonas campestris* pv. *vesicatoria*. *Journal of bacteriology* **191**, 1414-1428 (2009).
40. J. G. Kim, W. Stork, M. B. Mudgett, Xanthomonas type III effector XopD desumoylates tomato transcription factor SlERF4 to suppress ethylene responses and promote pathogen growth. *Cell host & microbe* **13**, 143-154 (2013).
41. A. U. Singer *et al.*, A pathogen type III effector with a novel E3 ubiquitin ligase architecture. *PLoS pathogens* **9**, e1003121 (2013).
42. S. Üstün, F. Börnke, The Xanthomonas campestris type III effector XopJ proteolytically degrades proteasome subunit RPT6. *Plant physiology* **168**, 107-119 (2015).
43. S. Üstün, V. Bartetzko, F. Börnke, The Xanthomonas effector XopJ triggers a conditional hypersensitive response upon treatment of N. benthamiana leaves with salicylic acid. *Frontiers in plant science* **6**, 599 (2015).
44. A. Hafrén, D. Hofius, NBR1-mediated antiviral xenophagy in plant immunity. *Autophagy* **13**, 2000-2001 (2017).
45. Q. Chai *et al.*, A Mycobacterium tuberculosis surface protein recruits ubiquitin to trigger host xenophagy. *Nature communications* **10**, 1973 (2019).
46. Y. T. Zheng *et al.*, The adaptor protein p62/SQSTM1 targets invading bacteria to the autophagy pathway. *J Immunol* **183**, 5909-5916 (2009).
47. J. Zhou *et al.*, NBR1-mediated selective autophagy targets insoluble ubiquitinated protein aggregates in plant stress responses. *PLoS Genet* **9**, e1003196 (2013).
48. G. Furlan *et al.*, Changes in PUB22 Ubiquitination Modes Triggered by MITOGEN-ACTIVATED PROTEIN KINASE3 Dampen the Immune Response. *The Plant cell* **29**, 726-745 (2017).
49. P. Albers, S. Üstün, K. Witzel, M. Kraner, F. Börnke, A Remorin from Nicotiana benthamiana Interacts with the Pseudomonas Type-III Effector Protein HopZ1a and is Phosphorylated by the Immune-Related Kinase PBS1. *Molecular plant-microbe interactions : MPMI* **32**, 1229-1242 (2019).
50. S. Üstün, P. Konig, D. S. Guttman, F. Börnke, HopZ4 from Pseudomonas syringae, a Member of the HopZ Type III Effector Family from the YopJ Superfamily, Inhibits the Proteasome in Plants. *Molecular plant-microbe interactions : MPMI* **27**, 611-623 (2014).
51. X. Zhuang *et al.*, A BAR-domain protein SH3P2, which binds to phosphatidylinositol 3-phosphate and ATG8, regulates autophagosome formation in Arabidopsis. *The Plant cell* **25**, 4596-4615 (2013).
52. X. Zhuang, L. Jiang, Autophagosome biogenesis in plants: roles of SH3P2. *Autophagy* **10**, 704-705 (2014).
53. M. K. Nagel *et al.*, Arabidopsis SH3P2 is an ubiquitin-binding protein that functions together with ESCRT-I and the deubiquitylating enzyme AMSH3. *Proceedings of the*

National Academy of Sciences of the United States of America **114**, E7197-E7204 (2017).

54. J. L. Erickson, N. Adlung, C. Lampe, U. Bonas, M. H. Schattat, The Xanthomonas effector XopL uncovers the role of microtubules in stromule extension and dynamics in Nicotiana benthamiana. *The Plant journal : for cell and molecular biology* **93**, 856-870 (2018).
55. Y. Jiao, J. Sun, Bacterial Manipulation of Autophagic Responses in Infection and Inflammation. *Front Immunol* **10**, 2821 (2019).
56. N. K. Kushwaha, A. Hafrén, D. Hofius, Autophagy-virus interplay in plants: from antiviral recognition to proviral manipulation. *Molecular plant pathology* **20**, 1211-1216 (2019).
57. B. Orosa *et al.*, Plant proteostasis - shaping the proteome: a research community aiming to understand molecular mechanisms that control protein abundance. *The New phytologist* **227**, 1028-1033 (2020).
58. A. Y. Leary *et al.*, Modulation of plant autophagy during pathogen attack. *Journal of experimental botany* **69**, 1325-1333 (2018).
59. J. G. Kim *et al.*, XopD SUMO protease affects host transcription, promotes pathogen growth, and delays symptom development in Xanthomonas-infected tomato leaves. *The Plant cell* **20**, 1915-1929 (2008).
60. G. Ahn *et al.*, SH3 Domain-Containing Protein 2 Plays a Crucial Role at the Step of Membrane Tubulation during Cell Plate Formation. *The Plant cell* **29**, 1388-1405 (2017).
61. Y. Gu, R. Zavaliev, X. Dong, Membrane Trafficking in Plant Immunity. *Molecular plant* **10**, 1026-1034 (2017).
62. H. D. Lenz *et al.*, Autophagy differentially controls plant basal immunity to biotrophic and necrotrophic pathogens. *The Plant journal : for cell and molecular biology* **66**, 818-830 (2011).
63. H. B. Yu *et al.*, Autophagy facilitates Salmonella replication in HeLa cells. *mBio* **5**, e00865-00814 (2014).
64. J. Huang *et al.*, Antibacterial autophagy occurs at PI(3)P-enriched domains of the endoplasmic reticulum and requires Rab1 GTPase. *Autophagy* **7**, 17-26 (2011).
65. F. Li *et al.*, Beclin1 restricts RNA virus infection in plants through suppression and degradation of the viral polymerase. *Nature communications* **9**, 1268 (2018).
66. F. Li *et al.*, A plant RNA virus activates selective autophagy in a UPR-dependent manner to promote virus infection. *The New phytologist* **228**, 622-639 (2020).
67. V. Kirkin, T. Lamark, T. Johansen, I. Dikic, NBR1 cooperates with p62 in selective autophagy of ubiquitinated targets. *Autophagy* **5**, 732-733 (2009).
68. F. S. Mesquita *et al.*, The Salmonella deubiquitinase SseL inhibits selective autophagy of cytosolic aggregates. *PLoS pathogens* **8**, e1002743 (2012).
69. L. Lou, P. Zhang, R. Piao, Y. Wang, Salmonella Pathogenicity Island 1 (SPI-1) and Its Complex Regulatory Network. *Frontiers in cellular and infection microbiology* **9**, 270 (2019).
70. T. Maculins, E. Fiskin, S. Bhogaraju, I. Dikic, Bacteria-host relationship: ubiquitin ligases as weapons of invasion. *Cell research* **26**, 499-510 (2016).
71. Y. Zhang, W. Higashide, S. Dai, D. M. Sherman, D. Zhou, Recognition and ubiquitination of Salmonella type III effector SopA by a ubiquitin E3 ligase, HsRMA1. *The Journal of biological chemistry* **280**, 38682-38688 (2005).
72. T. Kubori, J. E. Galan, Temporal regulation of salmonella virulence effector function by proteasome-dependent protein degradation. *Cell* **115**, 333-342 (2003).
73. G. Furlan, J. Klinkenberg, M. Trujillo, Regulation of plant immune receptors by ubiquitination. *Frontiers in plant science* **3**, 238 (2012).

74. J. R. Rohde, A. Breitkreutz, A. Chenal, P. J. Sansonetti, C. Parsot, Type III secretion effectors of the IpaH family are E3 ubiquitin ligases. *Cell host & microbe* **1**, 77-83 (2007).
75. J. Noad *et al.*, LUBAC-synthesized linear ubiquitin chains restrict cytosol-invading bacteria by activating autophagy and NF-kappaB. *Nat Microbiol* **2**, 17063 (2017).
76. Kovach, M., et. al., Four new derivatives of the broad-host-range cloning vector pBBR1MCS, carrying different antibiotic-resistance cassettes. *Gene* **166**, 175-6 (1995)
77. C. Grefen et al., A ubiquitin-10 promoter-based vector set for fluorescent protein tagging facilitates temporal stability and native protein distribution in transient and stable expression studies. *The Plant journal*: for cell and molecular biology **64**, 355-365 (2010).
78. T. Nakagawa et al., Development of series of gateway binary vectors, pGWBs, for realizing efficient construction of fusion genes for plant transformation. J Biosci Bioeng 104, 34-41 (2007).
79. S. J. Clough, A. F. Bent, Floral dip: a simplified method for Agrobacterium-mediated transformation of Arabidopsis thaliana. *The Plant journal*: for cell and molecular biology **16**, 735-743 (1998).
80. N. Borchert et al., Proteogenomics of *Pristionchus pacificus* reveals distinct proteome structure of nematode models. *Genome Res* **20**, 837-846 (2010).
81. K. Kliza et al., Internally tagged ubiquitin: a tool to identify linear polyubiquitin-modified proteins by mass spectrometry. *Nature methods* **14**, 504-512 (2017).
82. B. Schwanhausser et al., Global quantification of mammalian gene expression control. *Nature* **473**, 337-342 (2011).

Supporting information

Supplemental Figure 1

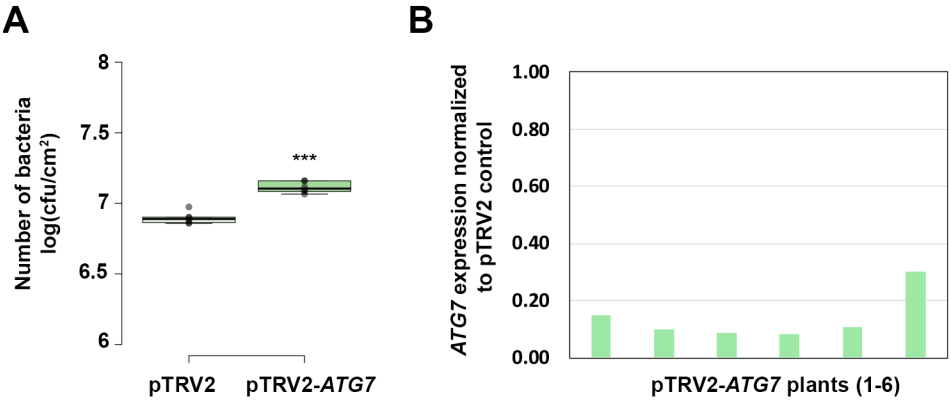

Fig. S1: Virus-induced gene silencing of *ATG7* in *N. benthamiana* plants.
(A) Growth of Xcv *ΔxopQ* in *N. benthamiana* plants silenced for *ATG7* (pTRV2-*ATG7*) compared to control plants (pTRV2). Leaves were syringe-inoculated with a bacteria suspension at OD_{600} = 0.0004 and bacteria were quantified at 9 dpi. Data represent the mean SD (n = 6). Significant differences were calculated using Student's *t-test* and are indicated by ***, P < 0.001. The experiment was repeated twice with similar trends.
(B) qRT-PCR analysis of *ATG7* mRNA levels in silenced pepper plants. *Actin* expression was used to normalize the expression value in each sample, and relative expression values were determined against pTRV2 control plants, which was set to 1.

Supplemental Figure 2

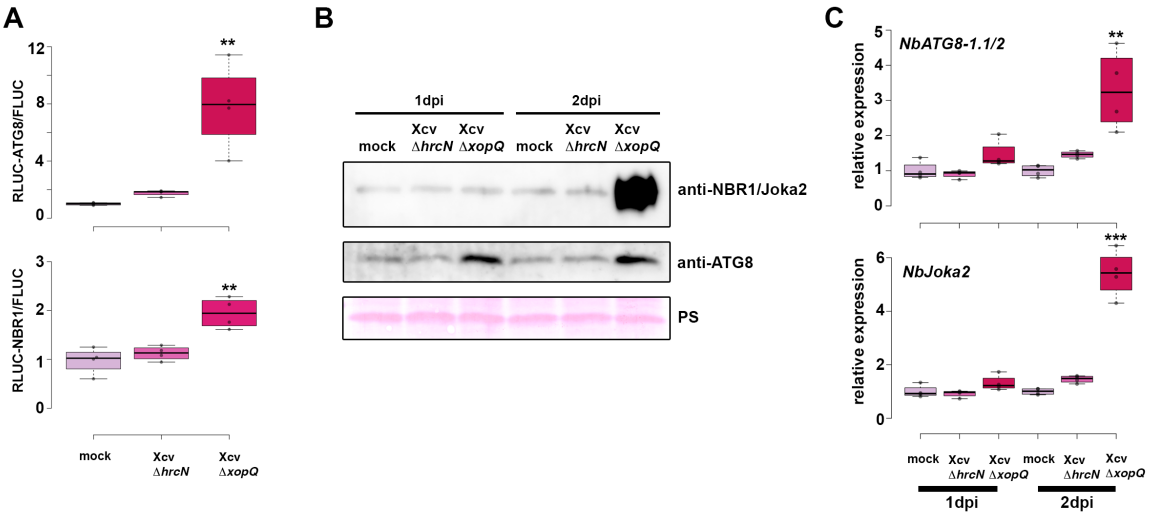

Fig. S2: Suppression of autophagy is enhanced by T3Es.

(A) Autophagic flux determined by quantitative dual-luciferase assay. RLUC-ATG8a or RLUC-NBR1 constructs were coexpressed with internal control FLUC in *N. benthamiana*. Xcv *ΔxopQ* and *ΔhrcN* were co-infiltrated with Agrobacteria containing the respective constructs. Renilla and Firefly luciferase activities were simultaneously measured in leaf extracts at 48 h post- infiltration using the dual-luciferase system. Values represent the mean ratio of RLUC-ATG8a and FLUC activities and error bars show SD (n=4). Statistical significance (***P*<0.01) was revealed by Student's *t*-test. The experiment was repeated 2 times with similar results.
(B) Immunoblot analysis of NBR1 and ATG8 protein levels in Xcv *ΔxopQ, ΔhrcN* or mock infected *N. benthamiana* plants at 1 and 2dpi. Ponceau Staining (PS) served as a loading control. The experiment was repeated twice with similar results.
(C) RT-qPCR analysis of *NbATG8-1.1/2, NbATG8-2.1/2* and *NbJoka2* transcript levels upon challenge of *N. benthamiana* plants with Xcv *ΔxopQ* and *ΔhrcN* for 1 and 2 dpi compared to mock infected plants. Values represent mean + SD (n=4) relative to mock control of respective time point and were normalized to *PP2A*. Statistical significance (***P* < 0.01, *** *P* < 0.001) was revealed by Student's *t*-test.

Supplemental Figure 3

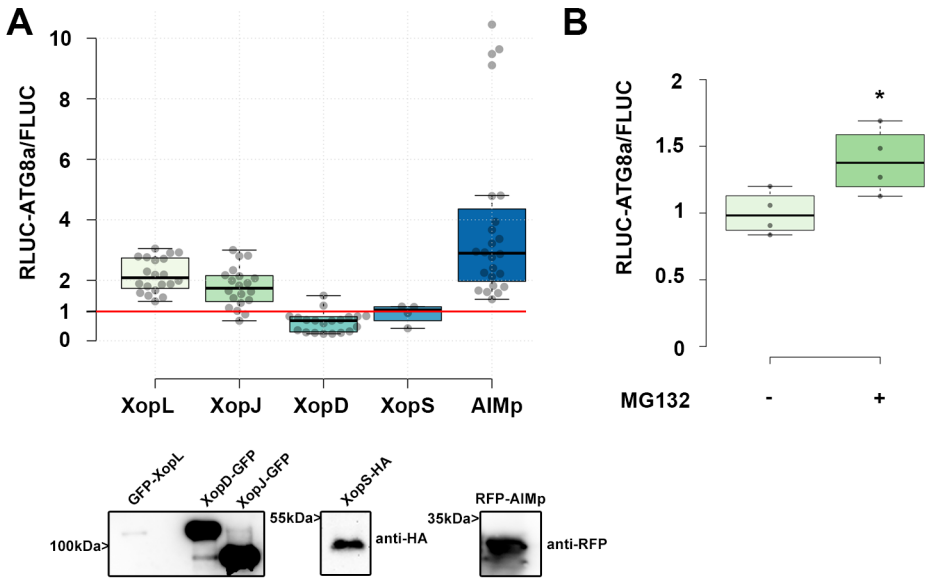

Fig. S3: Screening for Xanthomonas T3Es with altered autophagic flux.
(A) RLUC-ATG8a constructs were coexpressed with internal control FLUC in *N. benthamiana*. XopL, XopJ, XopD and XopS were co-infiltrated with the RLUC/FLUC mixture. Renilla and Firefly luciferase activities were simultaneously measured in leaf extracts at 48 h post-infiltration using the dual-luciferase system. Values represent the mean ratio of RLUC-ATG8a and FLUC activities and error bars show SD (XopL, XopJ, XopD, AIMp; n=20; XopS n=4). GFP served as a control and was set to 1 (red line). Expression of T3Es and RFP-AIMp were verified with the indicated antibodies. **(B)** RLUC-ATG8a constructs were coexpressed with internal control FLUC in *N. benthamiana*. Plants were treated with MG132 for 6 hours prior measurement. Values represent the mean ratio of RLUC-ATG8a and FLUC activities and error bars show SD (n=4). Statistical significance (* $P < 0.5$) was revealed by Student's *t*-test.

Supplemental Figure 4

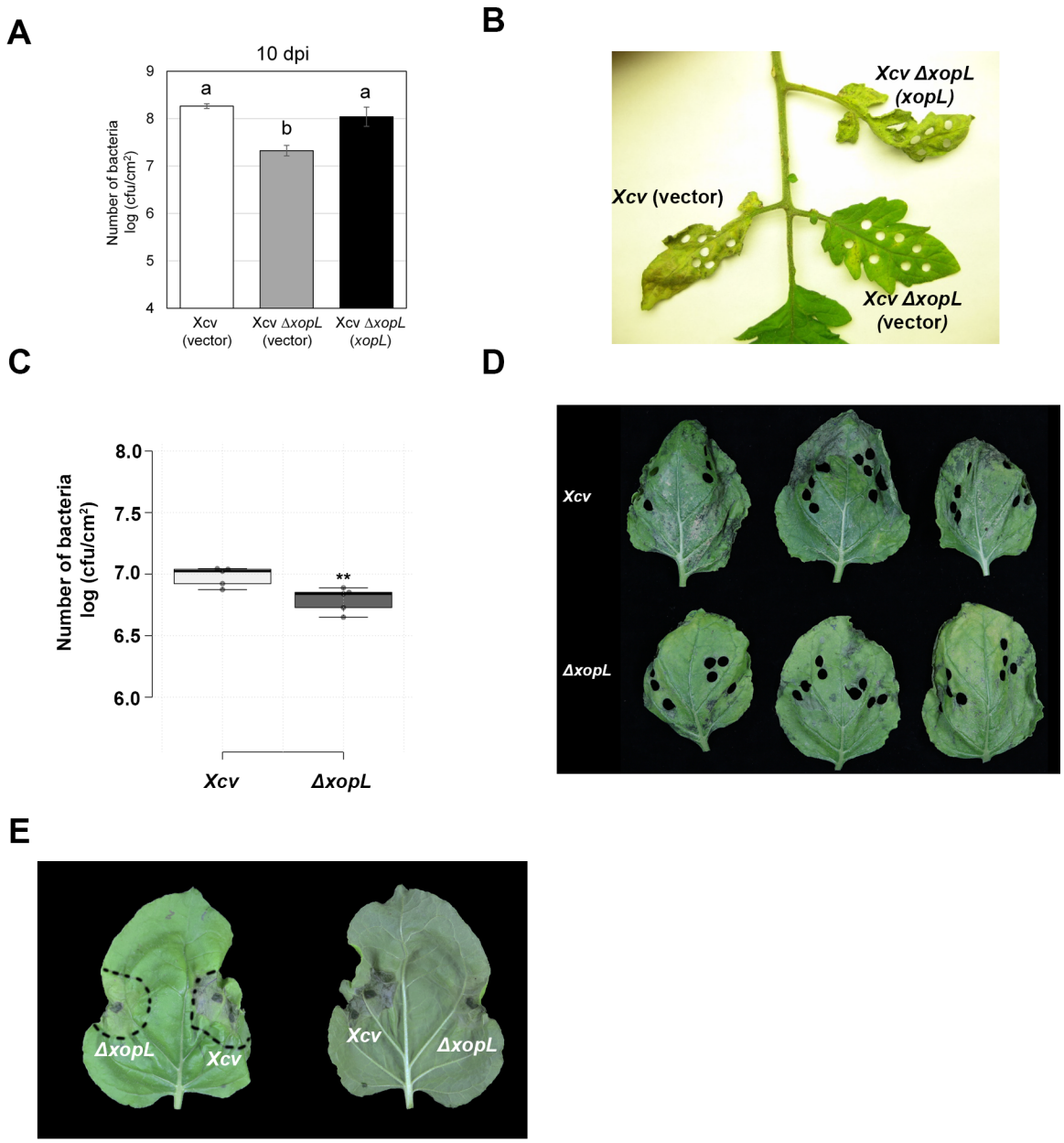

Fig. S4: XopL is an essential virulence factor
(A) Growth of Xcv 85-10 (vector) (white bar), Xcv 85-10 Δ*xopL* (vector) (grey bar), and Xcv 85-10 Δ*xopL* (*xopL*) (black bar) strains in tomato VF36 leaves. Leaves were dipped in a 2 x 10^8

CFU/mL suspension of bacteria. The number of bacteria in each leaf was quantified at 10 dpi. Data points represent mean $\log_{10}$ colony-forming units per cm^2 ± SD of three plants. Different letters above bars indicate statistically significant (Tukey's honestly significant difference (HSD) test, $P < 0.05$) differences between samples. Vector = pBBR1MCS-2.
(B) Delayed disease symptom development in tomato leaves inoculated with *Xcv* or *Xcv* Δ*xopL*. Tomato leaves inoculated with strains described in (A) were photographed at 14 dpi.
(C) Growth of Xcv 85-10, Xcv 85-10 Δ*xopL* strains in *roq1 N. benthamiana* leaves. Leaves were dipped in a 2 x 10^8 CFU/mL suspension of bacteria. The number of bacteria in each leaf was quantified at 10 dpi. Data represent the mean SD (n = 5). Significant differences were calculated using Student's *t-test* and are indicated by **, $P < 0.01$. The experiment was repeated twice with similar trends.

Supplemental Figure 5

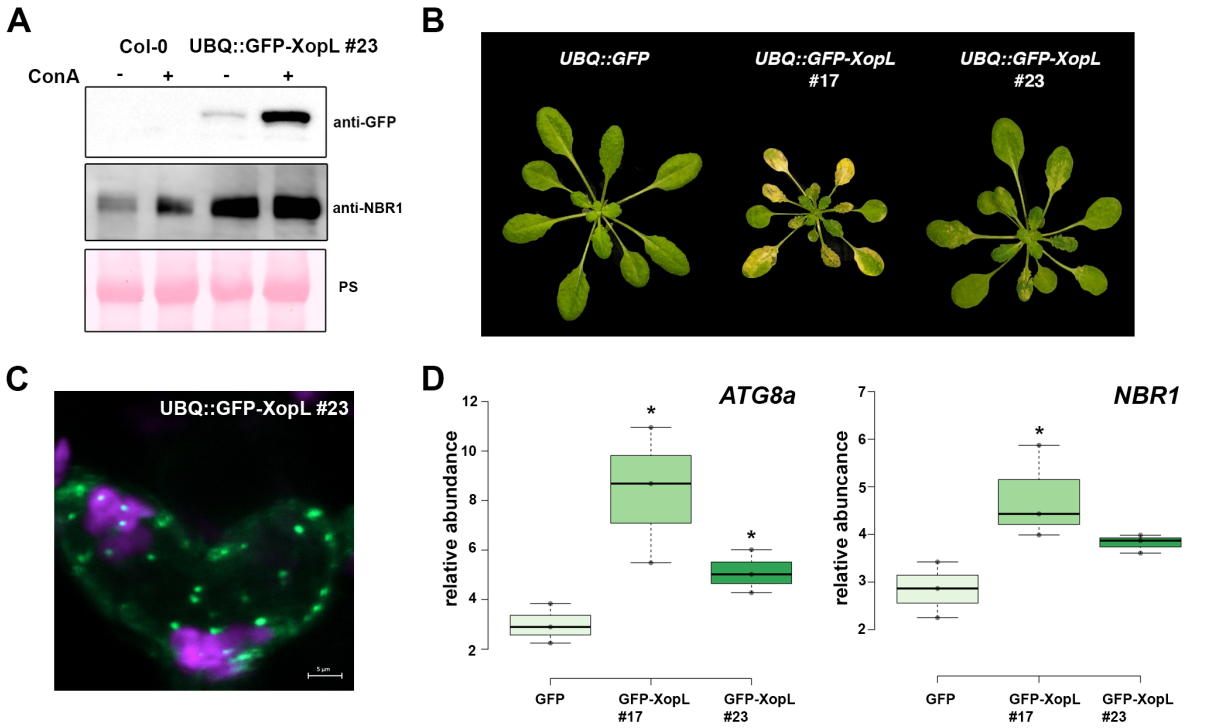

Fig. S5: Transgenic *A. thaliana* GFP-XopL plants display defects in autophagic degradation

(A) Immunoblot analysis of NBR1 protein levels in transgenic UBQ::GFP-XopL plants or Col-0. Plants were treated with concanamycin A (ConA) for 6 hours. Expression of GFP-XopL was verified with an anti-GFP antibody. Ponceau S staining serves as a loading control.
(B) 5 weeks old *A. thaliana* plants expressing UBQ::GFP-XopL develop an early senescence phenotype reminiscent of autophagy deficient mutants.
(C) Localization analysis of GFP-XopL of transgenic *A. thaliana* UBQ::GFP-XopL #23 line. Image represents single confocal planes from abaxial epidermal cells (bars = 5 µm).
(D) RT-qPCR analysis of *ATG8a* and *NBR1* transcript levels in *Arabidopsis thaliana* GFP or GFP-XopL plants. Values represent mean + SD (n=3) relative to GFP control and were normalized to *PP2A*. Statistical significance (**P*<0.05) was revealed by Student's *t*-test.

Supplemental Figure 6

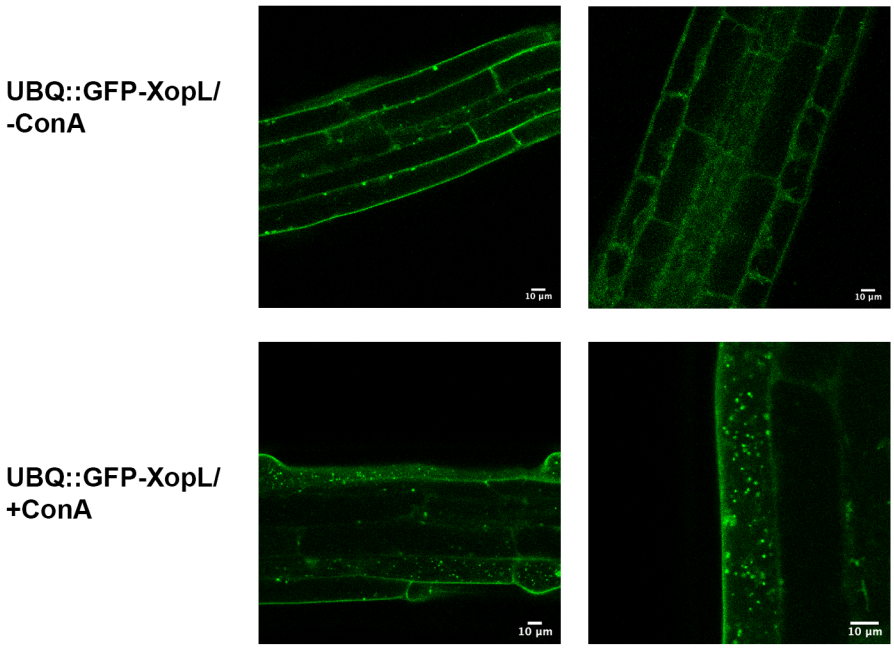

Fig. S6: XopL is degraded in the vacuole.
Localization of GFP-XopL in the presence or absence of ConA in transgenic GFP-XopL. DMSO or 0.5 µM ConA was used to treat seedlings, followed by confocal imaging of the roots. GFP-labeled puncta detectable upon ConA treatment indicate XopL accumulation in the vacuole (bars = 20 µm).

Supplemental Figure 7

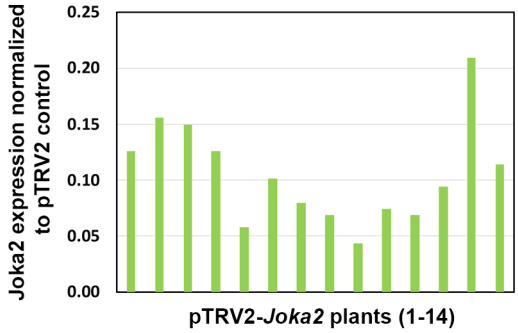

Fig. S7: Virus-induced gene silencing of *Joka2* in *N. benthamiana* plants. qRT-PCR analysis of Joka2 mRNA levels in *Joka2* silenced pepper plants. *Actin* expression was used to normalize the expression value in each sample, and relative expression values were determined against pTRV2 control plants (set to 1)**.**

Supplemental Figure 8

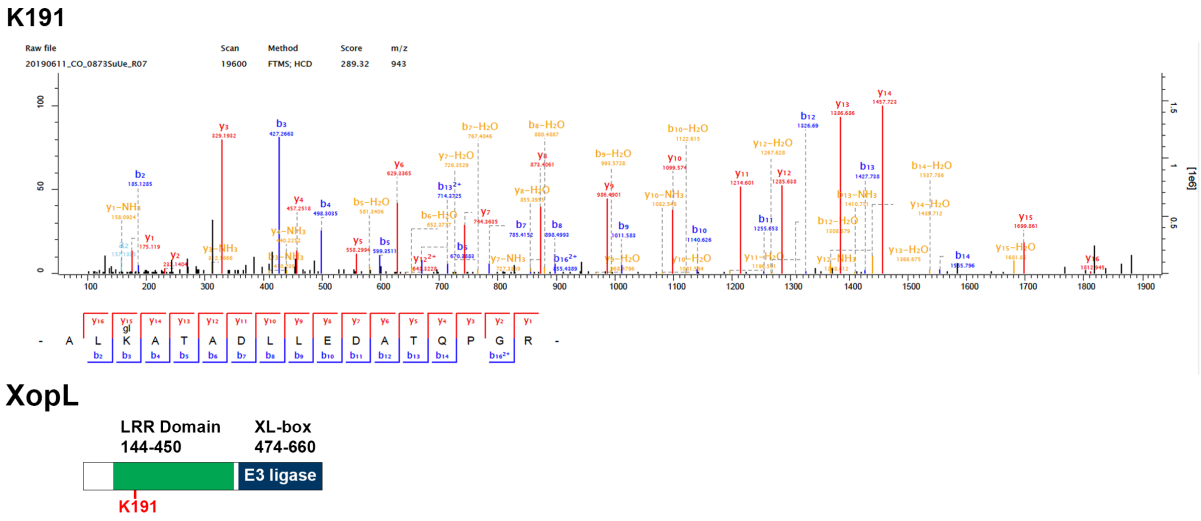

Fig. S8: XopL is ubiquitinated *in planta*.
XopL ubiquitination site at lysine 191 was identified in vivo by LC-MS/MS. GFP-XopL was transiently expressed in *N. benthamiana* and total proteins were subjected to anti-GFP IP followed by trypsin digestion. Ubiquitinated peptides were detected by LC-MS/MS. The spectrum shows the fragmentation pattern of the GlyGly modified peptide ALglKATADLLEDATQPGR corresponding to amino acids 189-205.

Supplemental Figure 9

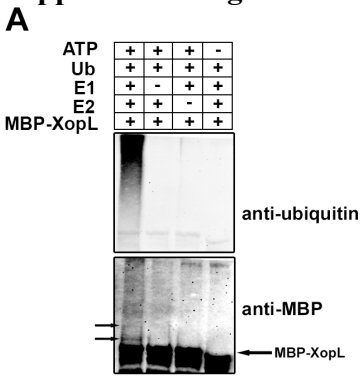

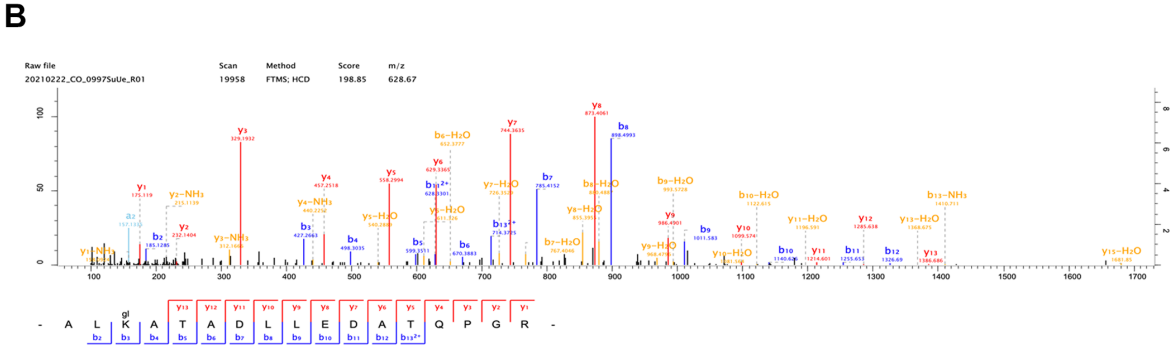

Fig. S9: XopL undergoes self-ubiquitination
(A) *In vitro* ubiquitination assay reveals autoubiquitination of XopL. Ubiquitination of MBP-XopL was tested using the Arabidopsis His-AtUBA1 and His-AtUBC8. Lanes 2 to 4 are negative controls. Proteins were separated by SDS-PAGE and detected by immunoblotting using the indicated antibodies. Arrows in the MBP blot indicate higher molecular weight bands

of MBP-XopL and autoubiquitination events. The experiment was repeated twice with similar results. **(B)** XopL ubiquitination site at lysine 191 was identified in vitro by LC-MS/MS. GST-XopL was used in an in vitro ubiquitination assay and samples were subjected to trypsin digestion. Ubiquitinated peptides were detected by LC-MS/MS. The spectrum shows the fragmentation pattern of the GlyGly modified peptide ALglKATADLLEDATQPGR corresponding to amino acids 189-205.

Supplemental Figure 10

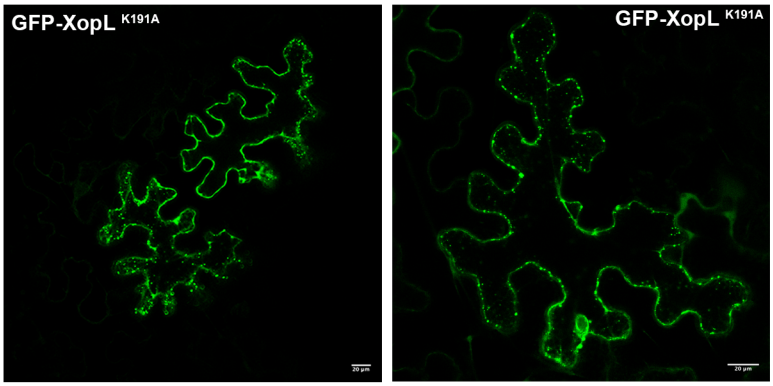

Fig. S10: Localization of GFP-XopL$_{K191A}$ in *N. benthamiana*.
Localization analysis of GFP-XopL$_{K191A}$ in *N. benthamiana* leaves. Imaging was performed 2 d after transient expression and images represent single confocal planes from abaxial epidermal cells (bars = 20 µm).

Supplemental Figure 11

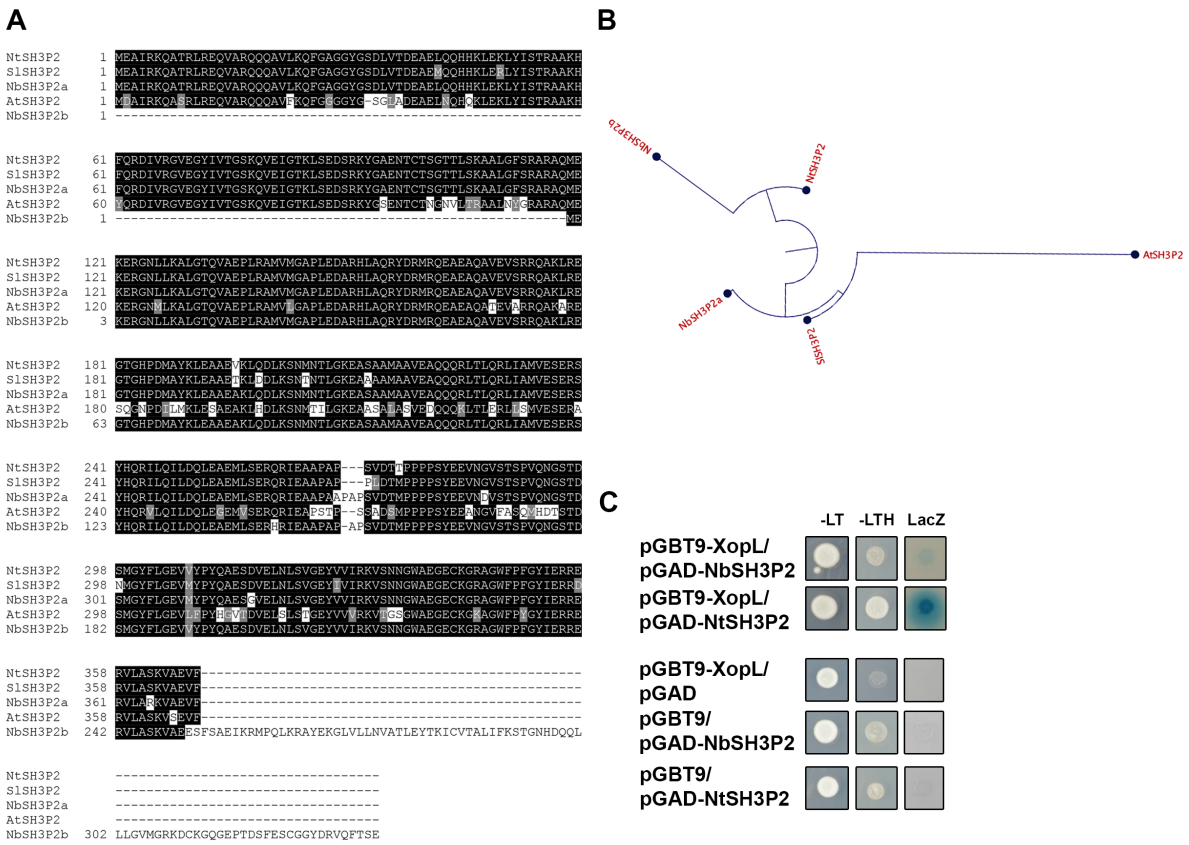

Fig. S11: SH3P2 is conserved in different plant species.
(A) Protein sequence alignment of SH3P2 from different species. The alignment was generated using CLUSTALW2 with default parameters and BoxShade 3.21. Positions of identical and similar sequences are boxed in black and grey, respectively. The following sequences were used to build the alignment: *Arabidopsis thaliana*, *Nicotiana tabacum, Nicotiana benthamiana*, *Solanum lycopersicum*. Phylogentic analysis of the SH3P2 from different plant species.
(B) XopL interacts with SH3P2 from *Nicotiana tabacum* and *Nicotiana benthamiana*. Interaction of XopL with SH3P2 in yeast two-hybrid assays. XopL fused to the GAL4 DNA-binding domain was expressed in combination with SH3P2 fused to the GAL4 activation domain (AD) in yeast strain Y190. Cells were grown on selective media before a LacZ filter assay was performed. The empty AD or BD vector served as negative control. NtSH3P2 = *Nicotiana tabacum* SH3P2, NbSH3P2 = *Nicotiana benthamiana* –LT = yeast growth on medium without Leu and Trp, –HLT = yeast growth on medium lacking His, Leu, and Trp, indicating expression of the HIS3 reporter gene. LacZ, activity of the lacZ reporter gene.

Supplemental Figure 12

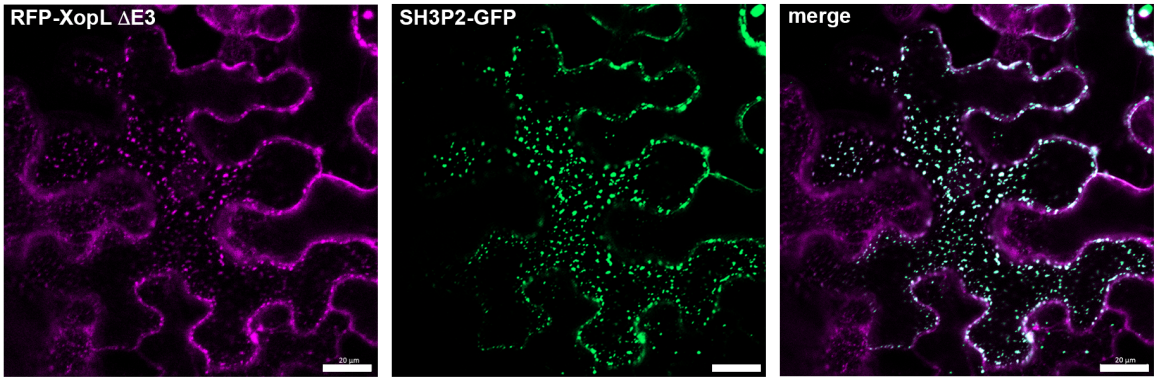

Fig. S12: RFP-XopL ΔE3 co-localizes with SH3P2-GFP.
Colocalization analysis of RFP-XopL ΔE3 with SH3P2-GFP in *N. benthamiana* leaves. Imaging was performed 2 d after transient expression and images represent single confocal planes from abaxial epidermal cells (bars = 20 µm).

Supplemental Figure 13

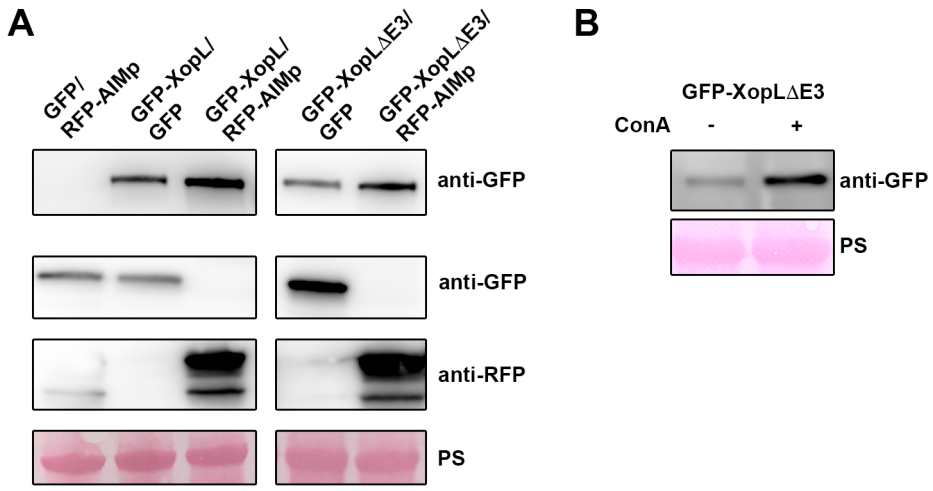

Fig. S13: Protein levels of GFP-XopL ΔE3 are stabilized by AIMp and ConA treatment.
(A) and (B) Immunoblot analysis of GFP protein levels using anti-GFP antibody. AIMPp was

verified by anti-RFP antibody. Plants were treated with concanamycin A (ConA) in (B) for 6 hours. Ponceau staining (PS) serves as a loading control.

Supplemental Figure 14

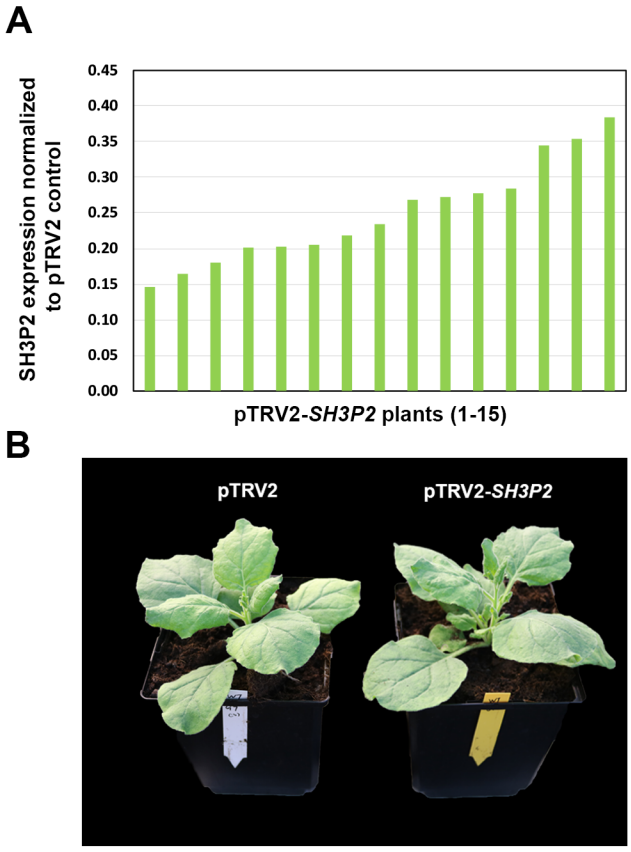

Fig. S14: Virus-induced gene silencing of SH3P2 in *N. benthamiana* plants. (A) qRT-PCR analysis of SH3P2 mRNA levels in silenced plants. *Actin* expression was used to normalize the expression value in each sample, and relative expression values were determined against pTRV2 control plants (set to 1)**. (B)** Phenotype of SH3P2-VIGS plants in comparison to the pTRV2 control. Picture was taken 14 dpi.

Supplemental Figure 15

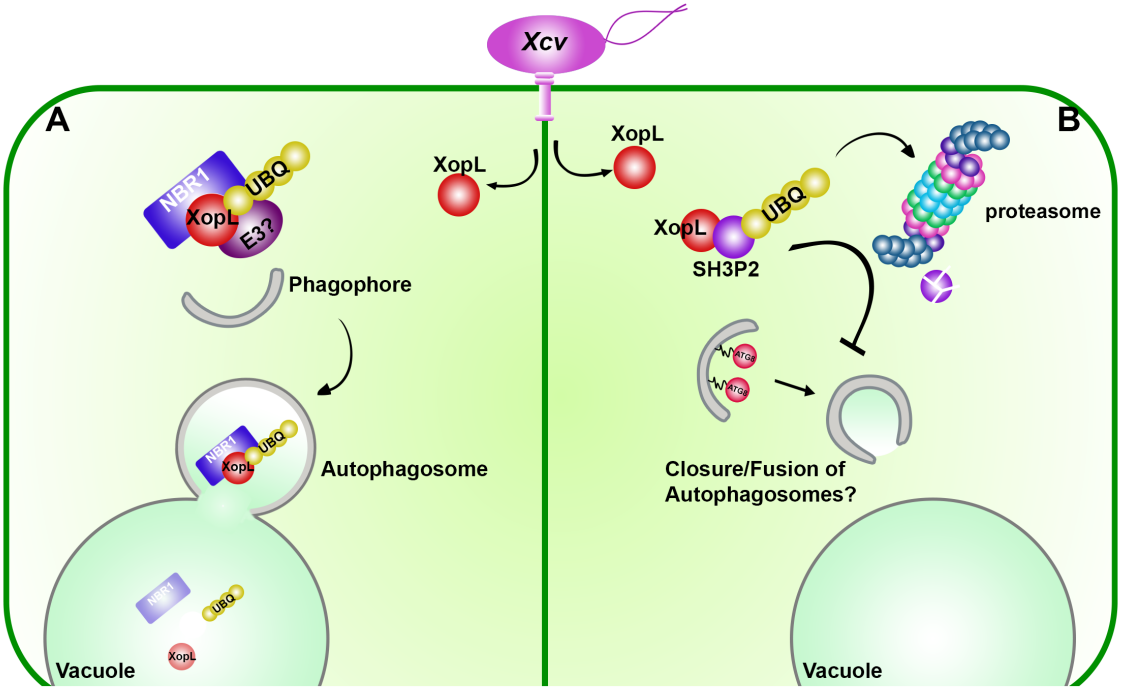

Fig. S15: Model illustrating the function of XopL

(A) Effectorphagy of XopL: Upon delivery of XopL in the plant XopL undergoes self-ubiquitination and possible ubiquitination by an unknown host E3 ligase. Joka2/NBR1 associates with XopL and triggers its degradation via the selective autophagy pathway "effectorphagy" in the vacuole. **(B) XopL blocks autophagy and self-degradation**: XopL interacts with autophagy component SH3P2 inside the cell and ubiquitinates it to degrade it via the 26S proteasome. Degradation of SH3P2 results in defects of autophagosome delivery into the vacuole and hence suppresses autophagy.